communications biology

A Nature Portfolio journal

Article

https://doi.org/10.1038/s42003-025-08135-3

Liver portal fibroblasts induce the functions of primary human hepatocytes in vitro

Grace E. Brown[1], Vedant V. Bodke[1], Brenton R. Ware[1,2] & Salman R. Khetani[1]

In vitro human liver models are critical to mitigate species-specific differences observed for toxicology, disease modeling, and regenerative medicine. Interactions with mesenchyme (i.e., fibroblasts) can promote phenotypic functions of primary human hepatocytes (PHHs) in culture; however, using liver-derived fibroblasts remains elusive. Portal fibroblasts (PFs) around the portal triad influence bile duct formation during development, but their role in regulating homeostatic hepatic functions remains unknown. Here, we show that human liver PFs induce long-term phenotypic functions in PHHs at higher levels than activated hepatic stellate cells across 2-dimensional and 3-dimensional culture formats. While PF-conditioned media induces some hepatic functions, partly via insulin-like growth factor binding protein-5 signaling, direct contact is necessary to induce optimal functional levels. Inhibiting Notch signaling reduces progenitor-like characteristics of PHHs and further enhances functionality. Overall, this work demonstrates a unique role for PFs in modulating hepatic functions and provides all-human and all-liver coculture strategies for downstream applications.

Owing to significant differences across species in liver drug metabolism pathways, in vitro models of the human liver are critical for (a) the investigations of drug clearance, metabolites, and liver injury; (b) elucidating the mechanisms of diseases such as metabolic dysfunction-associated steatotic liver disease (MASLD), alcoholic liver disease (ALD), hepatitis B virus (HBV) infection, and hepatocellular carcinoma for developing novel therapeutics; and, (c) cell-based therapies for patients suffering from end-stage liver failure[1,2]. Such models are fabricated using transformed cell lines, induced pluripotent stem cell (iPSC)-derived human hepatocyte-like cells (iHeps), and primary human hepatocytes (PHHs). However, transformed cell lines display abnormal proliferation and dysregulated liver functions, while protocols to further mature iHeps towards the adult PHH phenotype need improvement. In contrast, PHHs are the gold standard for modeling liver physiology and disease in vitro; however, liver functions rapidly decline when these cells are cultured on their own as 2-dimensional (2D) monolayers on plastic or glass, restricting their application use. Furthermore, PHH supply is limited due to a donor organ shortage; however, strategies to grow PHHs in vitro, as occurs during liver regeneration, are being actively pursued with some early success[3,4].

In vivo, the development of the liver necessitates the interaction of the endodermal hepatic bud with the surrounding mesenchyme[5]. Analogously, the cocultivation of hepatocytes with different mesenchymal cell types has been explored to prevent the functional decline of hepatocytes in vitro. Langenbach et al. reported that rat hepatocytes cultured on a feeder layer of irradiated C3H/10T1/2 mouse embryo cells maintained morphology and metabolism up to ~70% of fresh hepatocytes for 14 days[6]. Similarly, Guillouzo et al. demonstrated 40+ days of albumin secretion from rat and human hepatocytes upon coculture with rat liver epithelial cells[7,8]. Khetani et al. showed that various murine embryonic 3T3 fibroblast sub-clones could induce functions in rat hepatocytes, albeit 3T3-J2s were superior to NIH/3T3s and 3T3-L1s[9]. Khetani and Bhatia extended this work to PHHs, which displayed a stable phenotype for several weeks in vitro when micropatterned onto collagen-coated domains of empirically optimized dimensions to control homotypic interactions precisely and subsequently co-cultivated with 3T3-J2s[10]. These "micropatterned cocultures" (MPCCs) have proven to be highly useful for drug clearance prediction[11], drug metabolite profiling[12], drug-induced liver injury (DILI) assessment[13], infection with hepatitis B/C viruses[14,15] and malaria[16], and modeling critical dysfunctions in MASLD[17,18], such as steatosis, insulin resistance, fibrosis, and loss of hepatic drug metabolism and transport capacities. Furthermore, the MPCC platform has been augmented with human liver non-parenchymal cells (NPCs), such as liver sinusoidal endothelial cells[19], Kupffer cells[20], and hepatic stellate cells (HSCs)[17], to investigate various aspects of liver physiology and disease; however, none of the liver NPCs could induce hepatic functions to the same extent as the 3T3-J2s.

[1]Department of Biomedical Engineering, University of Illinois Chicago, Chicago, IL, USA. [2]School of Biomedical Engineering, Colorado State University, Fort Collins, CO, USA. e-mail: skhetani@uic.edu

While using murine embryonic fibroblasts is highly advantageous for inducing and stabilizing PHH functions for in vitro applications, it is unsuitable for regenerative medicine. Therefore, others have generated cocultures of PHHs with human fibroblasts. Stevens et al. utilized human dermal fibroblasts to induce PHH functions within spheroids[21]. Weaver et al. used unidentified human non-liver endothelia and non-liver stroma to induce PHH functions in 2D monolayers[22]. However, non-liver NPCs may be confounding for both in vitro and in vivo applications in which endogenous and exogenous molecules may be metabolized non-specifically. Therefore, there is a need for a coculture system containing PHHs and human liver-derived fibroblasts.

Liver portal fibroblasts (PFs) are located in the mesenchyme surrounding the bile ducts of the portal triad[23]. They contribute to fetal liver development by regulating the formation of bile ducts through molecules such as hedgehog and jagged ligands[24] that promote the differentiation of bipotential hepatoblasts toward the cholangiocyte lineage. PFs are also the major, if not the only, source of elastic fibers in the liver via the secretion of microfibril components, including fibrillin, fibulin-2, and elastin, which is critical for maintaining the structural stability of bile ducts[25,26]. However, thorough characterization of *human* PFs is not abundant in literature due to difficulties with isolation and identification[23]. Furthermore, the PF's role in supporting hepatic functions in or near the portal triad is unknown.

Here, we sought to first characterize immunostaining and gene expression patterns in passaged primary human PFs compared to passaged HSCs, as these cell populations are often compared due to their ability to differentiate into myofibroblasts in vitro and in vivo. Next, PFs were cocultured with PHHs in MPCCs or 3-dimensional (3D) spheroids to characterize their role in inducing PHH functions compared to HSCs. PFs and HSCs were also chemically growth-arrested to determine how the fibroblast to PHH ratio, including near physiologic, affects hepatic responses in vitro. The roles of paracrine and juxtacrine signaling in PHH + PF cocultures were further elucidated. Lastly, the roles of critical molecules in PF's effects on PHH functions were assessed using small interfering RNA (siRNA) technology and small molecule inhibitors of identified pathways. Overall, this study provides a unique framework for the epithelial-mesenchymal interactions that underlie the maintenance of PHH functions in the human liver while providing all-human and all-liver coculture strategies for downstream applications.

Results

PFs and HSCs express prototypical markers in vitro

At the gene expression level, passaged PFs expressed fibulin-2 (*FLBN2*), epidermal growth factor containing fibulin extracellular matrix protein 1 (*EFEMP1*), and thy-1 cell surface antigen (*THY1*) at 14.2-, 3.4-, and 3.6-fold higher levels, respectively, compared to passaged HSCs. HSCs expressed vasoactive intestinal polypeptide receptor 1 (*VIPR1*) at 271.2-fold higher levels than PFs. Both cell types expressed collagen 1α1 (*COL1A1*), vimentin (*VIM*), and alpha-smooth muscle actin (*α-SMA*) at similar levels (<2-fold) (Fig. 1A). Additionally, while both PFs and HSCs expressed collagen 1α1 and α-SMA proteins as assessed via immunostaining, fibulin-2 protein was expressed only by the PFs (Fig. 1B), consistent with published literature[23]. Lastly, both cell populations were devoid of endothelial cell or macrophage contamination, as verified via staining for cluster of differentiation 31 (CD31) and CD68, respectively (Supplementary Fig. 1); no PHH contamination was present either, as verified by visual inspection for prototypical hepatic morphology (PHHs do not survive passaging). Overall, the PF and HSC populations were 98–99% pure based on the markers assessed.

PFs were treated with transforming growth factor beta (TGF-β) and platelet-derived growth factor (PDGF)-BB and their small molecule inhibitors. TGF-β is known to exacerbate the activation of PFs[27]. Treatment with TGF-β led to an increase in α-SMA expression (Supplementary Fig. 2A) and an increase in PF proliferation based on 5-ethynyl-2′-deoxyuridine (EdU) positive nuclei (Supplementary Fig. 2B) and nuclei counts (Supplementary Fig. 2C) compared to untreated controls. While a statistically insignificant increase in PF proliferation was observed following treatment with PDGF-BB, no difference was observed in α-SMA expression compared to the untreated controls. Statistically insignificant decreases were seen in EdU-positive nuclei when treating PFs with chemical inhibitors of both TGF-β and PDGF-BB; however, no difference in total nuclei number was observed compared to the untreated control. Lastly, while PFs under passage 7 maintained contact inhibition, PFs over passage 7 began to grow atop each other and lose contact inhibition (Supplementary Fig. 3A). Furthermore, PFs at a higher passage 11 also secreted significantly more interleukin (IL)-6 protein than the PFs at passages 5 and 7, indicating a higher inflammatory phenotype at the higher passage (Supplementary Fig. 3B).

RNA sequencing analysis reveals further differences between PFs and HSCs

To further characterize key differences in PFs and HSCs, two donors each of PFs and HSCs were lysed, and bulk RNA sequencing was performed. While most genes were expressed at statistically similar levels (12,681 genes), 1024 genes were significantly upregulated in PFs, while 746 genes were upregulated in HSCs (Fig. 2A). Next, a differentially regulated pathway analysis was performed via the Reactome pathway database. The differentially expressed pathways upregulated in PFs included extracellular matrix (ECM) organization, elastic fiber formation, and regulation of insulin-like growth factor (IGF) transport and uptake by insulin-like growth factor binding proteins (IGFBPs) (Fig. 2B). In contrast, most of the pathways upregulated in HSCs are related to cell cycle regulation and DNA replication (Fig. 2C), likely due to their activated (myofibroblastic) state.

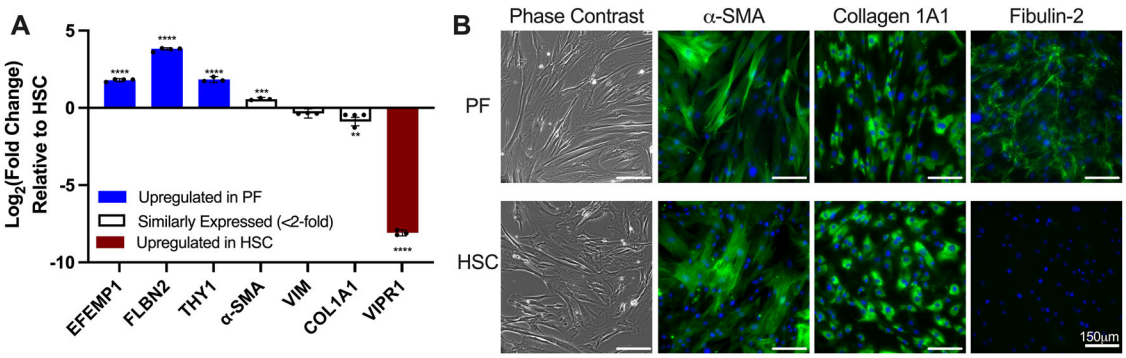

Fig. 1 | Gene expression and immunostaining patterns of PFs and HSCs. A PFs express certain genes at higher levels than HSCs (blue), including *EFEMP1*, *FLBN2*, and *THY1*. In contrast, *VIPR1* is expressed at a higher level in HSCs compared to PFs (red), while *α-SMA*, *VIM*, and *COL1A1* are expressed at similar levels (black) across both cell types (n = 3 or 4 technical replicates). **B** When cultured on tissue culture plastic, PFs and HSCs maintain an elongated, spindle-like morphology and express collagen 1a1 and α-SMA proteins, while only PFs express fibulin-2. Both PFs and HSCs are >98% pure based on these markers. Scale bar = 150 μm. $^{**}P < 0.01$, $^{***}P < 0.001$, $^{****}P < 0.0001$ between PF and HSC conditions.

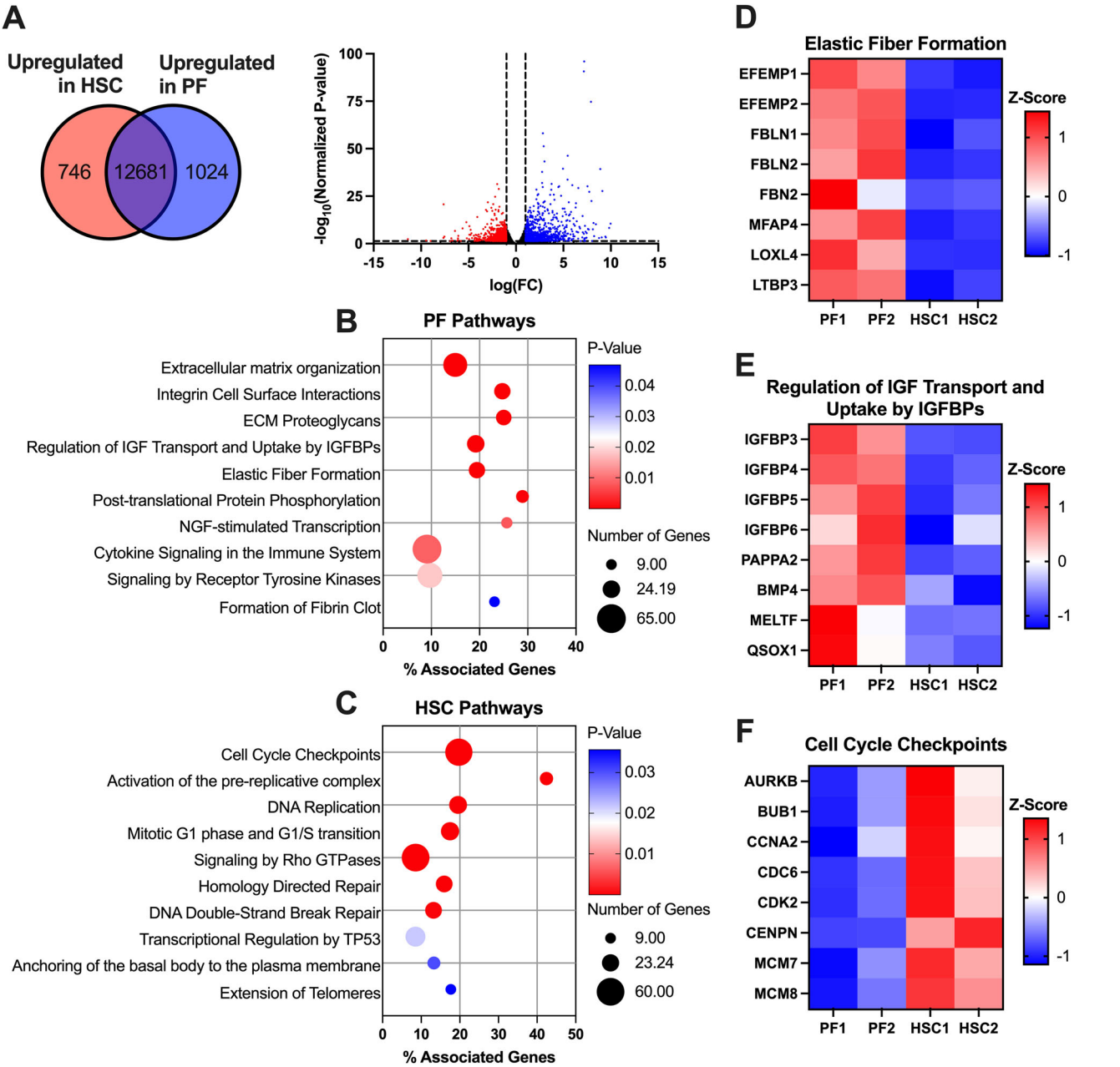

Fig. 2 | RNA sequencing analysis of PFs and HSCs. A Venn diagram depicting the number of differentially expressed genes between PFs and HSCs and volcano plot showing the spread of differentially expressed genes (red = upregulated in HSCs, blue = upregulated in PFs, and FC = fold change). Two donors for each cell type were used for sequencing, with two replicates per donor (n = 4 sequencing runs per cell type). **B** Reactome pathways that are differentially upregulated in PFs compared to HSCs. **C** Reactome pathways that are differentially upregulated in HSCs compared to PFs. Heatmap of key differentially expressed genes related to **D** elastic fiber formation, **E** regulation of IGF transport and uptake by IGFBPs, and **F** cell cycle checkpoints.

Specific genes related to differentially regulated pathways, including elastin fiber formation, regulation of IGF transport and uptake, and cell cycle checkpoints, were further analyzed for particular genes (Fig. 2D–F). In the elastic fiber formation pathway, various fibulins, including *FLBN1, FLBN2, EFEMP1* (also denoted *FLBN3*), and *EFEMP2* (also denoted *FLBN4*), were significantly upregulated in PFs compared to HSCs. Fibulin-1 and -2 are considered long fibulins, while fibulin-3 and -4 are considered short fibulins, all maintaining a role in ECM stabilization and fiber formation[28]. In the normal liver, thin elastic fibers are present in the portal region of the liver[26], verifying the role of PFs in elastic fiber formation. Elastin (*ELN*) itself was ~13-fold higher expressed on average in PFs than in HSCs from the sequencing data, albeit PF donor 1 had ~100-fold lower expression of *ELN* than PF donor 2.

In the pathway denoted "Regulation of IGF transport and uptake by IGFBPs," *IGFBP-3, -4, -5*, and *-6* were significantly increased in PFs compared to HSCs. In addition to binding IGFs to extend their half-life, IGFBPs have various independent biological effects[29]. For example, IGFBP5 can decrease lipid accumulation and improve insulin sensitivity in high-fat conditions[30]. Finally, multiple genes in the cell cycle checkpoint pathway, including *CCNA2*, which encodes for a cyclin that controls both the G1/S and G2/M transition phases, were significantly upregulated in HSCs compared to PFs, indicating a more proliferative cell population.

Other known markers of PFs[31,32] were also expressed at higher levels on average in PFs than HSCs, such as *CD34* (~10-fold), *CD200* (~3-fold), elastin microfibril interfacer 2 (*EMILIN2*, ~16-fold), and uroplakin-1b (*UPK1B*, ~4.6-fold); *CD105* was slightly (~1.4-fold) upregulated in PFs

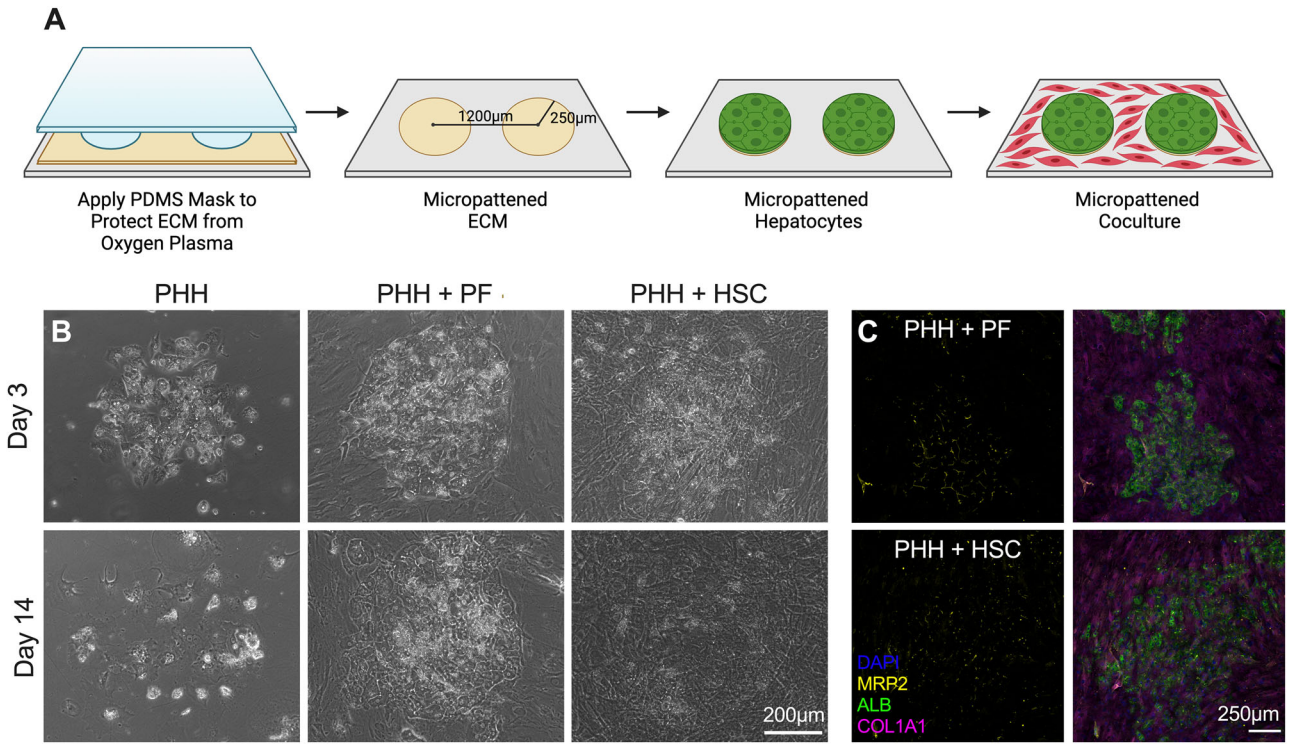

Fig. 3 | Morphology of MPCCs. A MPCCs were created by patterning collagen onto tissue culture polystyrene in multiwell plates using a soft-lithographic process. PHHs then selectively attach to the collagen circular domains, followed by seeding of the fibroblasts around the PHHs the next day. Created in BioRender. Khetani, S. (2025) https://BioRender.com/fqos6cx. **B** The morphology of the cultures was examined via phase contrast microscopy for PHH monocultures, PHH + PF MPCCs, and PHH + HSC MPCCs. **C** Bile canaliculi were visualized on day 21 via MRP2 (yellow) immunostaining. Localization was confirmed with albumin (green) for hepatocytes and collagen 1a1 (magenta) for fibroblasts. PHHs in coculture with PFs maintained prototypical morphology and island morphology better than the other two culture models. Scale bar = 200 μm for phase contrast images and 250 μm for immunostaining images.

than HSCs, while gremlin (*GREM1)* was expressed at similar levels in PFs and HSCs. Desmin (*DES*), an HSC marker, was expressed slightly higher (~1.7-fold) in PFs than HSCs; however, the expression levels were very low (~0.1% of *VIM*). Other HSC markers, such as lecithin retinol acyltransferase (*LRAT*), nerve growth factor receptor (*NGRF*), and glial fibrillary acidic protein (*GFAP*), were expressed at very low levels (filtered out during the normalization process) across both cell types, likely due to the myofibroblastic phenotype of the HSCs[33]. Similarly, the PF marker, ectonucleoside triphosphate diphosphohydrolase 2 (*ENTPD2)*, was expressed at very low levels across both cell types. These differences may be due to species variation from published literature[32] or passaging of PFs on plastic. Lastly, *VIM* was expressed at similar levels in both cell types, consistent with the reverse transcription and quantitative polymerase chain reaction (RT-qPCR) data (Fig. 1A). Overall, while some discrepancies were noted above with literature, the RT-qPCR, staining, and RNA sequencing analyses indicate that PFs retain most of their markers with passaging on plastic; at the same time, HSCs become myofibroblastic with similar passaging and lose key markers of quiescence.

PHH morphology, gene expression, and functions are better maintained upon coculture with PFs than HSCs in MPCCs

PHHs were patterned onto empirically optimized domains of collagen I to control homotypic interactions[10] and subsequently surrounded by either proliferative PFs or HSCs (3 fibroblasts:1 PHH) to create MPCCs, as illustrated in Fig. 3A. As expected, PHH monocultures rapidly de-differentiated and lost their prototypical polygonal morphology (Fig. 3B). In PHH + HSC cocultures, PHH colonies were invaded by proliferative and migratory HSCs, leading to disrupted homotypic interactions between neighboring PHHs. In contrast, PHH morphology and island integrity were maintained in PHH + PF cocultures. Lastly, the extent of bile canaliculi formation, as observed via immunostaining for a canalicular transport protein, multidrug resistance-associated protein 2 (MRP2), was enhanced in PHH + PF cocultures compared to PHH + HSC cocultures (Fig. 3C).

Gene expression of liver markers, including master transcription factors (Fig. 4A), nuclear receptors (Fig. 4B), drug transporters (Fig. 4C), and cytochrome P450 (CYP450) enzymes (Fig. 4D), was characterized in PHH + PF cocultures and compared to PHH + HSC cocultures over 3 weeks. Gene expression data were normalized to *GAPDH* and further normalized to PHH + PF cocultures at week 1 for each subsequent gene. Gene expression levels were higher in PHH + PF cocultures for all genes evaluated compared to PHH + HSC cocultures. For instance, PHH + PF cocultures had higher levels of *HNF4α* (4.5-fold), *HNF6* (2.7-fold), *CEBPα* (9.1-fold), *MRP2* (2.6-fold), *OATP1B1* (2.7-fold), *AHR* (1.9-fold), *PXR* (2.5-fold), *CAR* (2.4-fold), *CYP2D6* (16.6-fold), *CYP2E1* (107-fold), *CYP2B6* (2.9-fold), and *CYP2C19* (3.3-fold) than PHH + HSC cocultures.

As expected, albumin secretion rapidly declined in PHH monocultures to undetectable levels after 3 days (Fig. 5A). In contrast, albumin was detectable in the coculture supernatants for at least 21 days. However, albumin secretion was 1.8-, 3.6-, and 2.7-fold higher after 1, 2, and 3 weeks, respectively, in PHH + PF cocultures compared to PHH + HSC cocultures. As with albumin, urea secretion declined to negligible levels in PHH monocultures after a week (Fig. 5B). While urea levels were detectable in the supernatants of the PHH + HSC cocultures for 21 days, they were less than 1 μg mL^{-1} after 9 days. In contrast, after an initial decline of 50% between days 3 and 7, urea levels stabilized in PHH + PF cocultures to ~5–9 μg mL^{-1} for 21 days.

For CYP450 activities, PHH + PF cocultures had 19.3-fold higher CYP3A4 activity than PHH monocultures and 2.7-fold higher than PHH + HSC cocultures after 21 days (Fig. 5C). CYP2A6 activity in PHH + PF cocultures was 100-fold higher than PHH monocultures and 2.2-fold higher than PHH + HSC cocultures after 21 days (Fig. 5D). CYP2C9 activity in PHH + PF cocultures was 124-fold higher than PHH

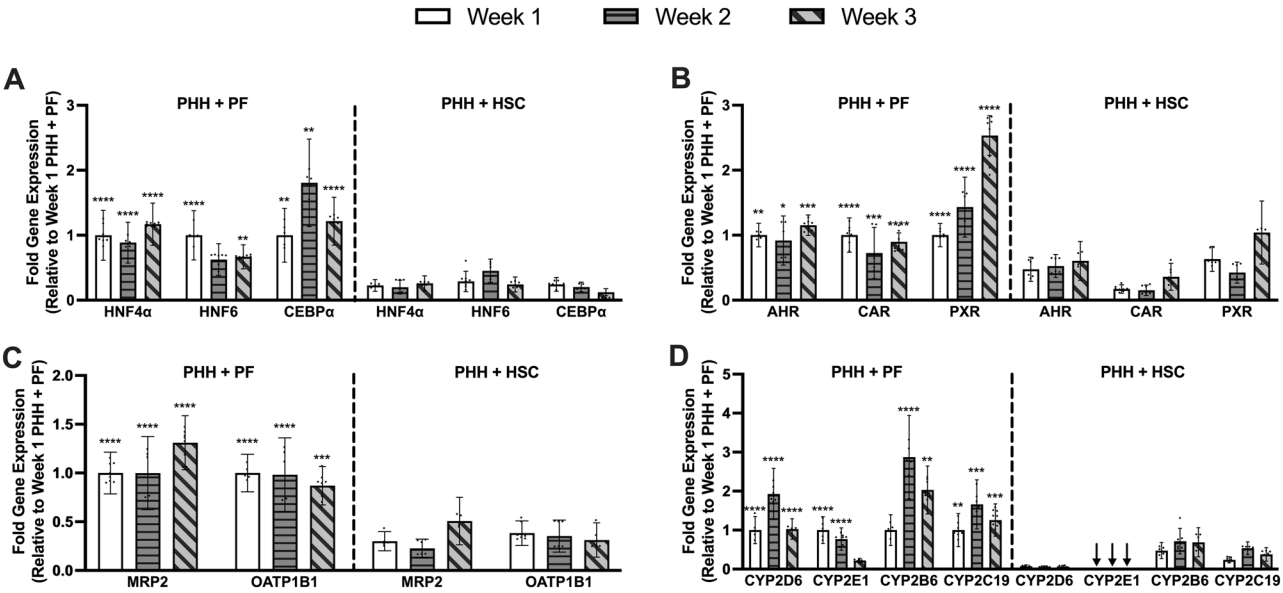

Fig. 4 | Gene expression patterns in MPCCs. Genes related to **A** master liver transcription factors, **B** nuclear receptors, **C** transporters, and **D** CYP450 enzymes were assessed at weeks 1, 2, and 3 of culture and normalized to values in PHH + PF MPCCs at week 1. Gene expression values were higher in PHH + PF versus PHH + HSC MPCCs. $^{*}P < 0.05$, $^{**}P < 0.01$, $^{***}P < 0.001$, $^{****}P < 0.0001$ between PHH + PF and PHH + HSC conditions. Arrows in (**D**) indicate values statistically similar to zero for CYP2E1 expression in PHH + HSC MPCCs (n = 5 to 8 technical replicates).

monocultures and 3.9-fold higher than PHH + HSC cocultures after 21 days (Fig. 5E). CYP1A2 activity in PHH + PF cocultures was 2-fold higher than PHH monocultures and 1.7-fold higher than PHH + HSC cocultures after 21 days (Fig. 5F). The results above show that proliferative PFs and HSCs can induce functions in PHHs, but PFs do so at a higher level over prolonged coculture.

Lastly, once cocultures were established, counting tightly packed PHHs in cocultures precisely over the entire duration of the culture and across all the wells became increasingly difficult. Furthermore, the extracted RNA was a mixture of the two cell types for the cocultures. Thus, no normalization of functional or gene expression data by PHH numbers, DNA, or protein was executed. Nonetheless, since the same number of PHHs were seeded across all models via precise cell patterning, any downregulation of hepatic gene expression and functions is likely due to the loss of PHH numbers via apoptosis or their dedifferentiation.

Chemically arresting the growth of PFs and HSCs still allows these cells to induce PHH functions

To decouple the effects of differences in PF and HSC growth rates from their ability to induce PHH functions, we determined the optimal concentrations of mitomycin C that growth-arrested PFs and HSCs without causing significant cell death; 2.5 μg mL^{-1} of mitomycin C was found to be optimal for PFs, and 5 μg mL^{-1} was found to be optimal for HSCs (Supplementary Fig. 4A, B). Next, we cocultured the growth-arrested fibroblasts with PHHs (1:1) while using the proliferative fibroblasts as control conditions. However, instead of the MPCC format, we utilized randomly distributed cocultures at a higher density of adherent PHHs (200K per well of a 24-well plate) versus the adherent density in MPCCs (30K per well). The rationale for this model selection was to ensure sufficient heterotypic contact between the PHHs and fibroblasts in coculture via the increase in cell number to 400K total per well (200 K for each cell type) as opposed to very sparse heterotypic contacts that would result at 1:1 fibroblast:PHH in MPCCs due to the PHH islands only covering ~10% of the surface area of the well.

PHH morphology was similar upon coculture with either growth-arrested or proliferative fibroblasts (Supplementary Fig. 4C). Similarly, PHH functions (albumin, urea, CYP3A4, CYP2A6) were similar upon coculture with either growth-arrested or proliferative fibroblasts (Supplementary Fig. 4D–G). Growth-arrested PFs also induced higher levels of hepatic functions than the growth-arrested HSCs, thereby suggesting that the rates of proliferations across the fibroblast types are not the sole mechanism underlying the differences in the variable induction of PHH functions.

When comparing the MPCC data (Fig. 5) to the random coculture data (Supplementary Fig. 4), we found that PFs induced up to ~1.8-fold higher albumin secretion than the HSCs in the random cocultures, which was lower than the 3.6-fold difference in MPCCs. PFs induced up to ~1.3-fold higher urea secretion than the HSCs in the random cocultures, which was lower than the ~13-fold difference in MPCCs. PFs induced up to ~2-fold higher CYP3A4 activity than the HSCs in the random cocultures, which was lower than the ~8.6-fold difference in MPCCs. Lastly, PFs induced up to ~1.5-fold higher CYP2A6 activity than the HSCs in the random cocultures, which was lower than the ~3-fold difference in MPCCs. Thus, these results indicate that the inductive effects of PFs on PHHs in MPCCs, which allow for controlled homotypic interactions between PHHs, 85% fewer adherent PHHs, and more significant heterotypic interactions (3 PF:1 PHH) than the random cocultures, are more pronounced than the inductive effects of HSCs on PHHs.

Reducing the fibroblast to PHH ratio to near physiologic also induces PHH functions

In the liver, the PHH to HSC ratio is ~12 to 1[34]. While the PHH to PF ratio in the liver is not known, it is most likely even lower than the PHH to HSC ratio, given the fewer numbers of PFs in the whole liver and restricted to the portal triad. With successful growth-arresting of both PFs and HSCs, we probed whether titrating the fibroblast numbers in cocultures could still induce PHH functions. Thus, we fabricated random cocultures containing 200K PHHs per well with varying numbers of growth-arrested fibroblasts (200K, 100K, 20K, and 10K), corresponding to fibroblast:PHH of 1:1, 1:2, 1:10, and 1:20, respectively. PHH monocultures were carried out as controls.

PHH monocultures declined in function, while all cocultures displayed higher functions. Increasing PF numbers generally induced higher urea levels (~3.7- to 17.7-fold after 15 days) than PHH monocultures; similarly, increasing HSC numbers induced higher urea levels (~8.6- to 17.6-fold after 15 days) (Supplementary Fig. 5A, B). Albumin levels dropped to undetectable levels after 7 days for PHH monocultures, whereas they increased over time in all cocultures. Increasing PF numbers induced albumin levels

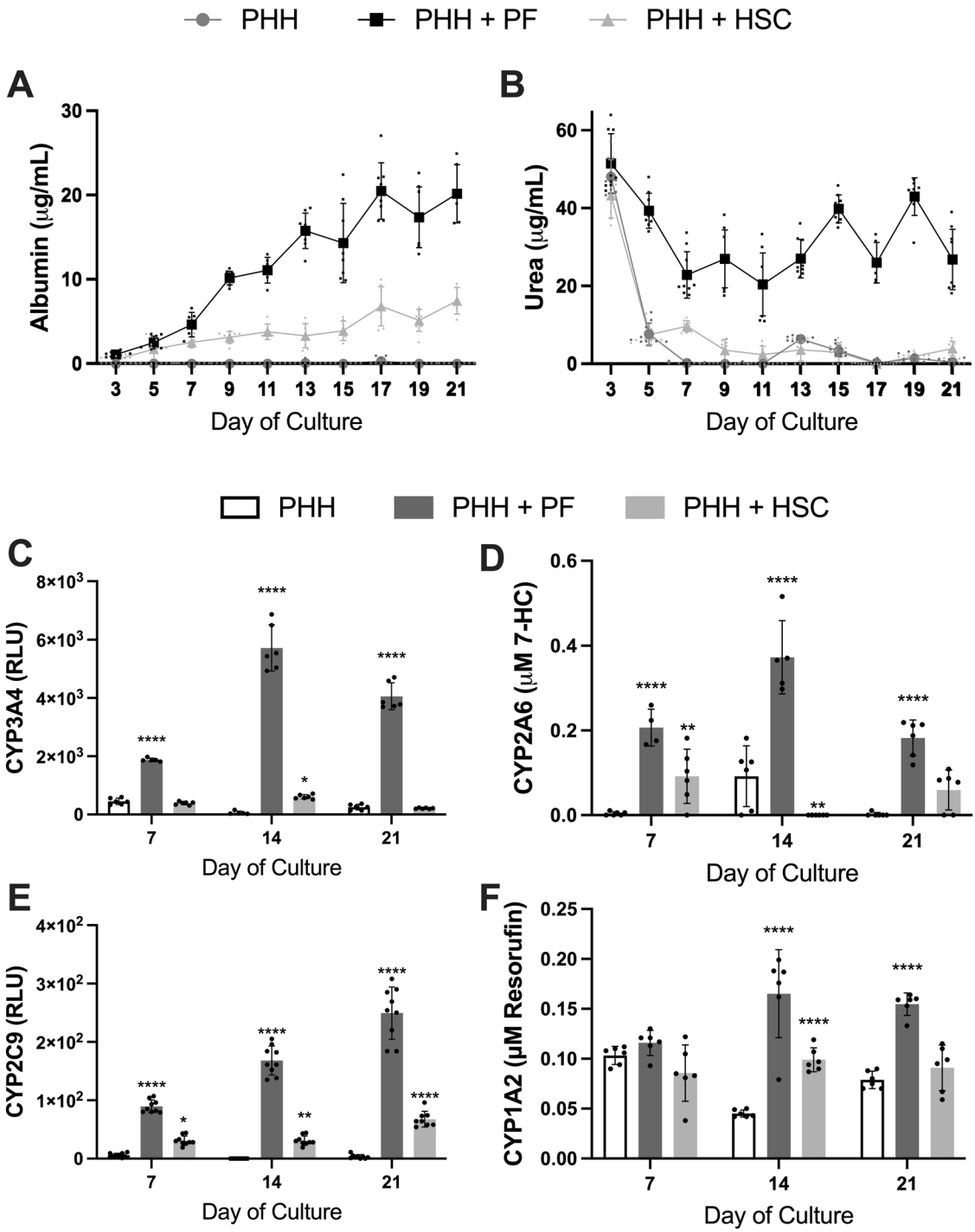

Fig. 5 | Hepatic functions of MPCCs. Time series of **A** albumin secretion (n = 8 technical replicates), **B** urea secretion (n = 9), **C** CYP3A4 enzyme activity (n = 6), **D** CYP2A6 enzyme activity (n = 6), **E** CYP2C9 enzyme activity (n = 9), and **F** CYP1A2 enzyme activity (n = 6) in MPCCs. Compared to the other culture models, functions were higher in PHH + PF MPCCs, especially after the first week. $^{*}P < 0.05$, $^{**}P < 0.01$, $^{***}P < 0.001$, $^{****}P < 0.0001$ with respect to the PHH monoculture control.

(~46- to 468-fold after 7 days) than PHH monocultures; similarly, increasing HSC numbers induced higher albumin levels (~85- to 496-fold after 7 days) (Supplementary Fig. 5C, D). For CYP450 activities, increasing PF numbers induced ~4.4- to 9.5-fold higher CYP3A4 activity and ~7.5- to 9-fold higher CYP2A6 activity than PHH monocultures after 15 days, while increasing HSC numbers induced ~3- to 5.4-fold higher CYP3A4 activity and ~7.1- to 10-fold higher CYP2A6 activity (Supplementary Fig. 5E–H). Therefore, even near physiologic ratios of PFs and HSCs can induce functions in PHHs, so long as the fibroblast growth is arrested and cell ratios are precisely controlled.

PFs, but not HSCs, can also induce PHH functions in 3D spheroids

Using 2D monolayers keeps the fibroblasts adhered to non-physiologic stiff plastic, which can be circumvented with self-aggregated spheroids, where cell-cell interactions allow the cells to form the junctions they need to

function. Thus, we cultured cells within non-adhesive molded agarose microwells in a 24-well plate format to form self-assembled spheroids of 100-250 μm diameters[35], as illustrated in Fig. 6A. The fibroblasts were not growth-arrested for these experiments to enable comparison with the MPCC data.

Cultures containing only PHHs formed larger spheroids (200-250 μm) compared to coculture conditions where the fibroblastic cells caused contraction of the PHH spheroids (Fig. 6B). Similar functional trends in MPCCs were also observed in spheroids; however, functions were 5- to 100-fold lower in spheroids than in MPCCs when accounting for differences in PHH seeding numbers, potentially due to the disorganized mixing of the cells in the spheroids as opposed to precise patterning and thus controlled cell-cell interactions in MPCCs. Nonetheless, albumin secretion in PHH + PF coculture spheroids was 2.5-fold higher than PHH monoculture spheroids and 14-fold higher than PHH + HSC coculture spheroids after 21 days (Fig. 6C). Urea secretion in PHH + PF coculture spheroids was 1.5-fold higher than PHH monoculture spheroids and 1.7-fold higher than PHH + HSC coculture spheroids after 21 days (Fig. 6D). CYP3A4 activity in PHH + PF coculture spheroids was 2-fold higher than PHH monoculture spheroids and 1.8-fold higher than PHH + HSC coculture spheroids after 21 days (Fig. 6E). CYP2A6 activity in PHH + PF coculture spheroids was 2.3-fold higher than PHH monoculture spheroids and 2.7-fold higher than PHH + HSC coculture spheroids after 14 days; however, activities were statistically similar and low for the three models on day 21 (Fig. 6F). CYP2C9 activity in PHH + PF coculture spheroids was 2.6-fold higher than PHH monoculture spheroids and 3.6-fold higher than PHH + HSC coculture spheroids after 21 days (Fig. 6G). Lastly, CYP1A2 activity in PHH + PF coculture spheroids was 3.3-fold higher than PHH monoculture spheroids and 2-fold higher than PHH + HSC coculture spheroids after 14 days; however, activities were statistically similar and low for the three models on day 21 (Fig. 6H).

The data above shows that while the exact fold change levels differ across MPCCs and spheroids, PFs induce PHH functions across 2D and 3D platforms, which is useful for both in vitro (e.g., drug screening, disease modeling) and in vivo (e.g., cell-based therapy) applications. Interestingly, HSCs did not induce PHH functions significantly in spheroids (and, in some cases, caused even lower hepatic functions than PHH monoculture spheroids). In contrast, HSCs induced PHH functions on plastic in both MPCCs and random cocultures, suggesting that their behavior/secretions in spheroids may not be the same as on plastic.

Higher passages of PFs and HSCs can also be used to induce PHH functions when TGF-β signaling is inhibited

To determine the passage dependency of PFs in their ability to support PHHs, cocultures were created using passage 5, 7, or 11 PFs. PHH island integrity and morphology were severely disrupted by the overgrowth of passage 11 PFs (Supplementary Fig. 6A). Such morphological changes correlated with higher IL-6 secretion from cocultures containing passage 11 PFs (Supplementary Fig. 6B). At the functional level, albumin secretion levels and kinetics were not significantly affected by the passage number of PFs (Supplementary Fig. 6C). However, urea secretion levels in the cocultures with passage 11 PFs were ~40% and ~25% of the urea levels in cocultures with passage 7 and 5 PFs, respectively, after 21 days (Supplementary Fig. 6D). CYP3A4 activities in the cocultures with passage 11 PFs were ~40% and ~30% of the CYP3A4 activity in cocultures with passage 7 and 5 PFs, respectively, after 22 days (Supplementary Fig. 6E). Lastly, CYP2A6 activities in the cocultures with passage 11 PFs were ~30% and ~11% of the CYP2A6 activity in cocultures with passage 7 and 5 PFs, respectively, after 22 days (Supplementary Fig. 6F).

Including an inhibitor of the TGF-β pathway (SB431542, blocks TGF-β receptor I)[36] in the culture medium of cocultures improved hepatic morphology and island integrity with passage 11 PFs (Supplementary Fig. 6A). IL-6 levels in the cocultures containing passage 11 PFs were reduced to 22-55% by SB431542 treatment compared to untreated controls but were still ~3–7-fold higher than in cocultures containing passage 5 and 7 PFs (Supplementary Fig. 6B). Even with such incomplete reduction in IL-6 levels, urea secretions were statistically similar across all cocultures treated with SB431542 for the 3 weeks (Supplementary Fig. 6D); in contrast, albumin secretions were statistically similar only in the third week of coculture (Supplementary Fig. 6C). CYP3A4 activities were statistically similar across all cocultures treated with SB431542 in the second and third week (Supplementary Fig. 6E), while CYP2A6 was ~80% in passage 11 PF cocultures compared to the lower passage cocultures after 3 weeks (Supplementary Fig. 6F). Therefore, inhibition of TGF-β signaling can partially reduce inflammation in cocultures containing higher passage PFs and rescue some PHH functions over time to similar levels as those with lower passage PFs.

PHH + HSC cocultures were also treated with SB431542. They showed similar improvements in some PHH functions (albumin CYP3A4, CYP2A6, and MRP2 protein expression) versus the untreated controls (Supplementary Fig. 7) as that seen with PHH + PF cocultures (Supplementary Fig. 6). Thus, hepatic functions can be enhanced across both coculture models via the inhibition of TGF-β signaling.

PF-conditioned media can also induce PHH functions but not to the same level as in direct contact (juxtacrine) coculture

To determine if direct cell-cell contact from PFs is required to induce PHH functionality, PHH monocultures were treated with conditioned media (CM) from PFs. PF CM significantly improved hepatic morphology compared to PHH monocultures and to a similar extent as PHH + PF cocultures (Fig. 7A). Likewise, albumin was secreted at a similar level and with similar kinetics in PHH + PF CM compared to the PHH + PF cocultures, especially after 2 weeks (Fig. 7B). In contrast, while hepatic urea secretion was induced by PF CM by up to 6.5-fold, it was 2-fold lower than in PHH + PF cocultures after 21 days (Fig. 7C). As with urea, PF CM induced CYP450 activities in PHH monocultures compared to untreated controls but at lower levels than the PHH + PF cocultures. Specifically, PF CM induced CYP3A4 activity in PHH monocultures by 1.7-fold compared to untreated controls but was 58% of the activity in PHH + PF cocultures after 21 days (Fig. 7D). As with CYP3A4 activity, PF induced CYP2C9 activity in PHH monocultures by 1.9-fold compared to untreated controls but was 55% of the activity in PHH + PF cocultures after 21 days (Fig. 7F). For CYP2A6 (Fig. 7E) and CYP1A2 (Fig. 7G), induction of activities by PF CM was minimal (e.g., 1.2- to 1.3-fold and not statistically significant for the majority of the time series) compared to untreated controls; however, PHH + PF cocultures induced up to 2.2-fold higher CYP2A6 activity and up to 1.5-fold higher CYP1A2 activity compared to untreated PHH monocultures. Therefore, PF CM can induce albumin to the same extent as juxtacrine coculture but not the other PHH functions measured.

IGFBP5 is involved in insulin signaling in cocultures of PFs and PHHs

Insulin sensitivity is a crucial regulator of various liver functions, including lipid and glucose metabolism[37]. To determine if PHH + PF cocultures could maintain insulin sensitivity compared to PHH monocultures and PHH + HSC cocultures, culture wells were divided into two groups and treated with media containing gluconeogenic substrates (lactate and pyruvate) with or without insulin; glucose production was subsequently assessed. The ratio of the glucose output in wells without insulin to those with insulin was calculated with values closer to zero denoting insulin sensitivity while values closer to 1 denoting insulin resistance[18,38]. While PHH + PF cocultures maintained a ratio between 0.1 and 0.2 during the 3-week culture period, PHH monocultures and PHH + HSC cocultures maintained a significantly higher ratio with values ranging from 0.55 to 1.3, indicating that PHH + PF cocultures can remain sensitive to insulin compared to other culture conditions (Fig. 8A).

Previous studies have shown that IGFBP5 plays a role in insulin sensitivity, specifically under MASLD conditions, through increasing the phosphorylation of insulin receptor substrate 1 (IRS1) on tyrosine residues and decreasing phosphorylation on serine residues[30]. As IGFBP5 was found

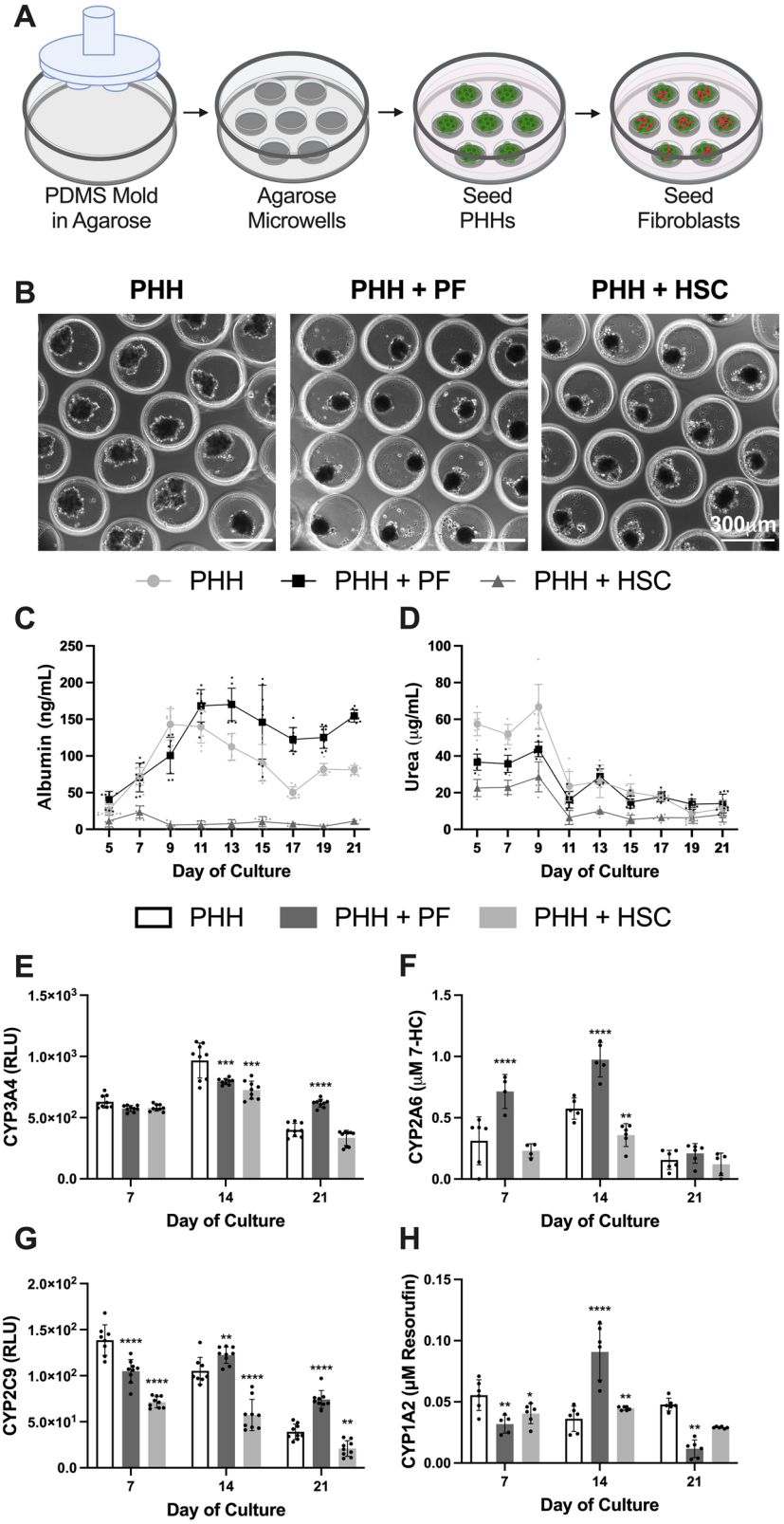

Fig. 6 | Hepatic functions of spheroids. **A** Spheroids were created by seeding PHHs into agarose microwells molded using a polydimethylsiloxane (PDMS) stamp and adding fibroblasts. Created in BioRender. Khetani, S. (2025) https://BioRender.com/6ngy08a. **B** The morphology of the spheroids was assessed via phase contrast on day 14 of the culture. Scale bar = 300 μm. Time series of **C** albumin and **D** urea secretion in spheroid cultures (n = 6 or 9 technical replicates). Time series of **E** CYP3A4 (n = 9), **F** CYP2A6 (n = 6), **G** CYP2C9 (n = 9), and **H** CYP1A2 enzyme activities (n = 6). $^{*}P < 0.05$, $^{***}P < 0.001$, $^{****}P < 0.0001$ between the PHH monoculture condition and PHH + PF or PHH + HSC coculture conditions.

to be increased in PFs compared to HSCs based on the RNA sequencing analysis (Fig. 2E), this difference was verified using RT-qPCR, which revealed a 2.9-fold increase in IGFBP5 expression in PFs compared to HSCs (Fig. 8B).

Next, the role of PF-derived IGFBP5 in PHH insulin sensitivity was assessed. Therefore, siRNA-mediated gene knockdown was performed directly in cocultures to target IGFBP5, and efficiency was evaluated by measuring the secreted protein in the supernatant. While a non-specific decrease was observed between the untreated control and the scrambled siRNA-treated control on day 14, by day 19, these controls were statistically similar. However, in the IGFBP5 siRNA-treated cultures, the levels of IGFBP5 protein secretion dropped closer to zero (Fig. 8C). The near

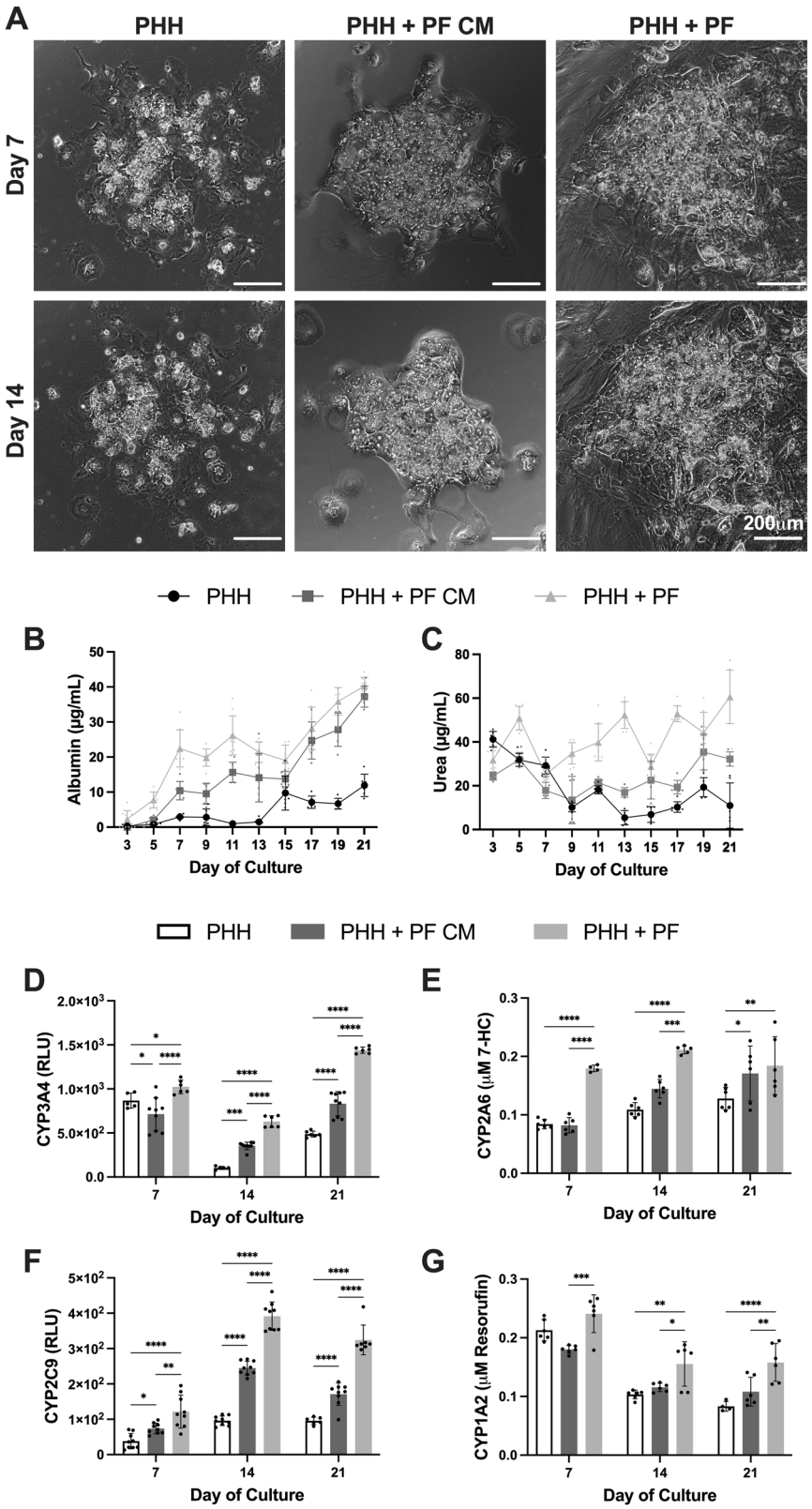

Fig. 7 | Effects of paracrine and juxtacrine PF interactions on PHHs. A Phase contrast images of PHH + PF CM showed improvement in prototypical PHH morphology compared to PHH-only de-differentiated cultures; additionally, PHH morphology in PHH + PF CM was qualitatively like that in PHH + PF cocultures with juxtacrine interactions between the two cell types. While **B** albumin secretion was at a similar level in PHH + PF CM compared to PHH + PF cocultures, **C** urea secretion was higher in PHH + PF cocultures (n = 6 technical replicates for PHH and PHH + PF CM and n = 9 for PHH + PF). Furthermore, while **D** CYP3A4 (n = 6 technical replicates for PHH and PHH + PF and n = 9 for PHH + PF CM), **E** CYP1A2 (n = 6), and **F** CYP2C9 (n = 9) enzyme activities increased in PHH + PF CM by at least the second week of culture compared to PHH-only cultures, the activities in PHH + PF CM remained lower than PHH + PF cocultures. Lastly, **G** CYP1A2 enzyme activity was not increased in PHH + PF CM but increased in PHH + PF cocultures compared to the PHH-only cultures (n = 6). $^{*}P < 0.05$, $^{**}P < 0.01$, $^{***}P < 0.001$, $^{****}P < 0.0001$, ns not significant.

complete knockdown of IGFBP5 protein secretion was also observed in PF monocultures (Supplementary Fig. 8C), suggesting that the siRNA can act directly on the PFs. At the gene expression level in cocultures, IGFBP5 was decreased by 13.9-fold compared to untreated controls and 10.3-fold compared to the scrambled siRNA-treated control at 11 days post-transfection; in contrast, the expression of other genes involved in glucose update and insulin sensitivity, namely *GLUT2, IRS1*, and *FOXO1*, were not affected in a statistically distinguishable manner compared to the scrambled siRNA-treated controls (Supplementary Fig. 8A).

All coculture conditions above remained highly functional as no statistically significant differences were detected for either albumin (Fig. 8D) or urea (Supplementary Fig. 8B) secretions, suggesting that these functions are

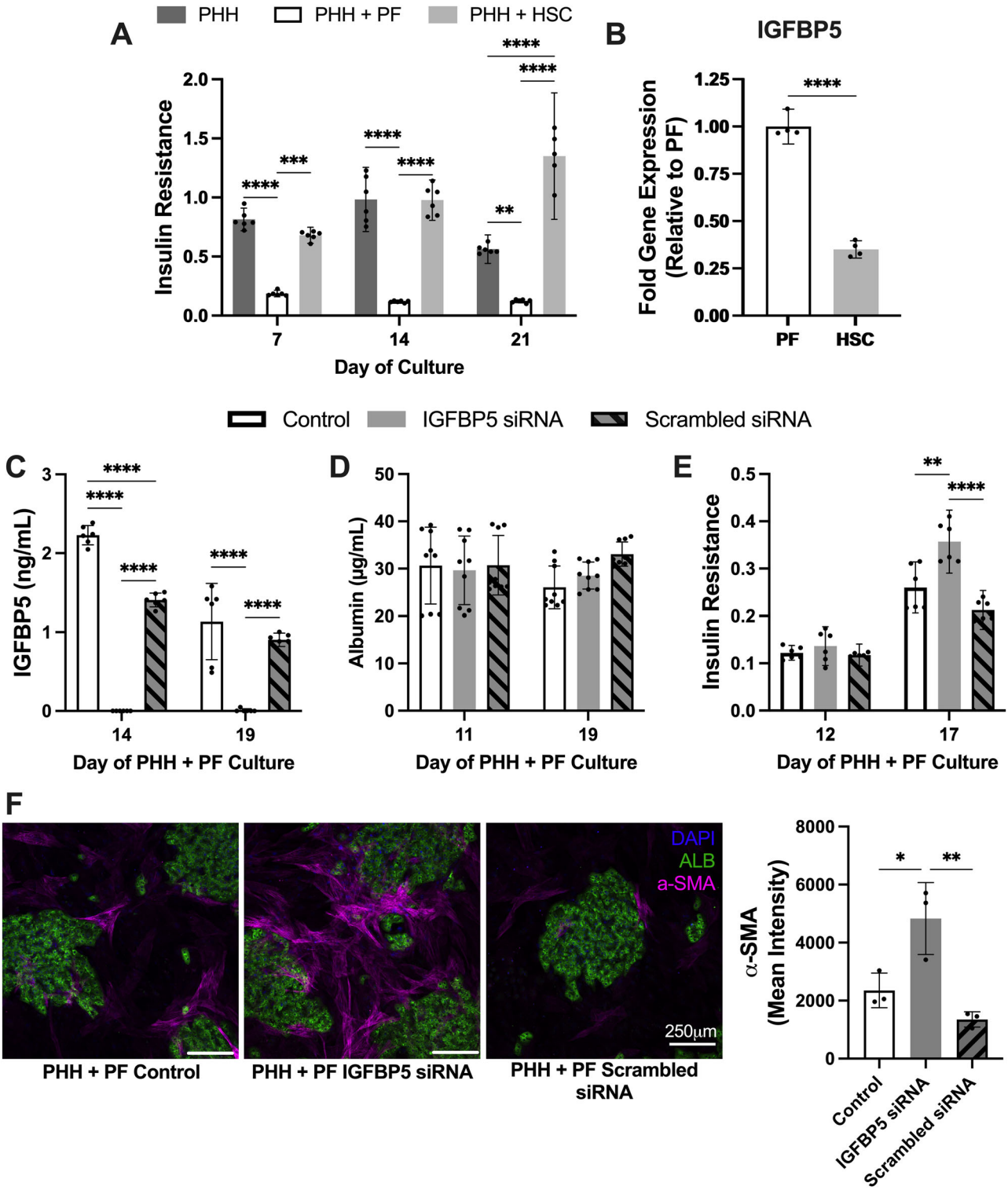

Fig. 8 | Insulin resistance/sensitivity and the effects of IGFBP5 in MPCCs. **A** Insulin resistance in MPCCs over time, as assessed by taking the ratio of glucose production by the cultures with or without insulin, with a value of "1" indicating complete insulin resistance while a value of "0" indicating complete insulin sensitivity or no insulin resistance. Compared to the other culture models, insulin resistance was lower (and insulin sensitivity was higher) in PHH + PF MPCCs (n = 6 technical replicates). **B** IGFBP5 gene expression was higher in PFs compared to HSCs (n = 4). **C**–**F** Treatment of PHH + PF MPCCs with IGFBP5 siRNA after 7 days of culture led to **C** downregulation of secreted IGFBP5 (n = 6 replicates), **E** no change in albumin secretion (n = 9), but **D** higher insulin resistance compared to untreated (control) or scrambled siRNA-treated MPCCs (n = 6). Additionally, **F** the α-SMA protein expression increased in IGFBP5 siRNA-treated PHH + PF MPCCs compared to the control treatments without affecting albumin expression (n = 3). Quantification of the staining intensity is to the far right. $^{*}P < 0.05$, $^{**}P < 0.01$, $^{***}P < 0.001$, $^{****}P < 0.0001$ Scale bar = 250 µm.

not affected by IGFBP5 signaling (or the increased PF activation via IGFBP5 knockdown as discussed below). However, insulin resistance in IGFBP siRNA-treated cocultures was increased 1.4-fold compared to untreated controls and 1.7-fold compared to scrambled siRNA-treated controls at 10 days post-transfection (Fig. 8E).

It has been shown that the overexpression of IGFBP5 attenuates biliary fibrosis in models of mouse cholestatic liver injury[39], indicating that IGFBP5 may provide an autocrine signaling pathway to decrease myofibroblastic characteristics. Therefore, IGFBP5 siRNA-treated and control PHH + PF cocultures were immunostained for α-SMA, and the mean staining intensity was quantified (Fig. 8F). The staining intensity for α-SMA increased in IGFBP5 siRNA-treated cocultures by 2-fold compared to untreated controls and 3.6-fold compared to scrambled siRNA-treated controls, suggesting the role of IGFBP5 in decreasing PF activation in an autocrine manner.

Inhibition of Notch signaling improves PHH functions in coculture with PFs or HSCs

PFs can express the Notch ligand, Jagged-1, which interacts with Notch-1 and -2 and causes gamma-secretase cleavage, enabling downstream notch signaling[25,40] (Fig. 9A). Notch signaling contributes to biliary development and maintenance and, when inhibited, leads to less dense and stunted elongation of the biliary tree[41]. In another study, Notch signaling led to a more biliary-like phenotype[42]. Thus, here, the role of Notch signaling between PFs and PHHs in cocultures was tested using the gamma-secretase inhibitor, DAPT (*N*-[*N*-(3,5-Difluorophenacetyl)-L-alanyl]-*S*-phenylglycine *t*-butyl ester)[41]. With the addition of DAPT to the culture medium, a 2.7-fold decrease in the downstream Notch target, Hes1, was observed compared to the untreated controls (Supplementary Fig. 9A). Likewise, genes related to a progenitor-like phenotype, including *CK19*, *CD115*, and *PTX3*, were decreased by 3.9-, 3.9-, and 5.2-fold, respectively, in DAPT-treated cocultures compared to untreated controls (Supplementary Fig. 9B).

For PHH functions, DAPT treatment caused transient decreases in albumin secretion from PHH + PF cocultures compared to untreated controls, albeit albumin continued to increase over 21 days in both conditions (Fig. 9B). However, urea secretion was not affected by DAPT treatment in PHH + PF cocultures (Fig. 9C). While hepatic morphology was not affected by DAPT treatment, the extent of bile canaliculi formation was enhanced with DAPT treatment compared to untreated controls, as observed via immunostaining for MRP2 (Fig. 9D). Lastly, CYP450 activities were upregulated in DAPT-treated PHH + PF cocultures compared to the untreated controls. Specifically, CYP3A4 activity was enhanced 20- to 22-fold (Fig. 9E), and CYP2A6 activity was enhanced 3- to 9-fold (Fig. 9F) over 3 weeks in DAPT-treated cocultures compared to the untreated controls. Another gamma-secretase inhibitor, compound E[43], was used to validate increases in CYP450 activities in PHH + PF cocultures compared to the untreated controls (Supplementary Fig. 10).

PHH + HSC cocultures treated with DAPT responded similarly as the PHH + PF cocultures such that the extent of bile canaliculi formation, CYP3A4 activity (~7-fold after 21 days), and CYP2A6 activity (~3.6-fold after 21 days) were all enhanced compared to untreated controls, while albumin and urea secretion were not significantly affected (Supplementary Fig. 7). Thus, hepatic functions can be enhanced across both coculture models via Notch pathway inhibition.

Discussion

We found key similarities between human PFs isolated here and previously published data in rodent PFs, such as *EFEMP1*, *FBLN2*, and *THY1* expression[23]. RNA sequencing analysis was used to identify additional differences between passaged PFs and HSCs. While most genes were expressed at statistically similar levels, PFs expressed genes related to elastic fiber formation (e.g., *MFAP4*, *FBN2*, *EFEMP1*). Thin elastic fibers are found around the portal areas of the normal liver and the liver capsule to provide structural support[26]. Specifically, MFAP4 localizes around the mesenchyme surrounding the bile ducts in human liver slices[44], which indicates PF's key role in synthesizing ECM proteins to maintain the structural integrity of the liver. PFs upregulated expression of genes related to IGF signaling, such as *IGFBP3, -4, -5*, and *-6*, which may modulate hepatocyte functions. Insulin-like growth factor-I (IGF-I), predominantly secreted by hepatocytes, circulates in a tertiary complex with IGFBPs, most commonly with IGFBP3 and -5. Pregnancy-associated plasma protein A2 (PAPPA2) is a metalloprotease that is required to cleave IGF-I from IGFBP3 and IGFBP5 to increase the bioavailability of IGF-I[45]. As PFs express both *IGFBPs* and *PAPPA2*, they may play a key role in modulating cellular phenotype through IGF signaling, which has been found in the liver to modulate mitochondrial function, inflammation, and insulin signaling[45]. Compared to PFs, HSCs increased expression of cell cycle checkpoints (e.g., *AURKB*, *CCNA2*, *CDC6*); passaged HSCs also minimally expressed quiescent phenotype markers, such as *DES* and *GFAP*.

The RNA sequencing analysis also revealed higher expression of other known PF markers[31,32], such as *CD34, CD200, EMILIN2*, and *UPK1B*, compared to HSCs; however, *CD105* and *GREM1* were not higher, and *ENTPD2* was expressed at very low levels across both cell types. The reasons for some of the discrepancies above with literature are unclear but could be either due to species differences or the effects of PF passaging on plastic. Nonetheless, the RT-qPCR, immunostaining, and RNA sequencing analysis collectively indicate that PFs retain most of their markers with passaging, though HSCs become myofibroblasts. Lastly, other fibroblast types in the liver exist, such as the connective tissue surrounding the extrahepatic bile ducts and capsular fibroblasts[23]. We cannot entirely rule out the presence of these fibroblasts in our preparations due to the lack of distinguishing markers; nonetheless, the preparations are highly pure (98–99%) for the staining markers we evaluated here.

We used micropatterning of PHHs to precisely control their homotypic interactions across the various mono- and coculture conditions. Compared to de-differentiating PHH monocultures, passaged HSCs caused some upregulation of albumin and CYP450 enzyme activities, consistent with previous literature[17,46–48], which suggests that even with passaging HSCs retain some of their physiological ability to modulate the PHH phenotype. However, passaged HSCs did not induce PHH functions to the same magnitude and longevity as PFs, which induced functions via juxtacrine (direct contact) and paracrine interactions. Notably, direct contact with PFs was required for the highest induction of PHH functions. Further studies are needed to elucidate the role of contact molecules, such as cadherins[9], in this coculture effect.

While substrate stiffness alone is critical for HSC activation in vitro, a combination of substrate stiffness and stimulation with cytokines, such as TGF-β, is required for PF activation[27,33]. Here, we verified that stimulating PFs with exogenous TGF-β led to increased proliferation and expression of α-SMA. Thus, PF activation may not occur to the same extent as HSC activation in the diseased liver, or certainly not with the same kinetics/progression. Indeed, lineage tracing in mice shows that HSCs give rise to 82% to 96% of fibrogenic myofibroblasts in 7 different models of liver fibrosis, including model systems targeting the biliary region[49]. Based on in vivo marker tracing studies, it has also been suggested that PFs may be the first stabilizing responders to the onset of biliary injury but do not cause significant disease progression to fibrosis[50]. While freshly isolated quiescent HSCs may further induce PHH functions than activated (passaged) HSCs, such cells are unavailable commercially as vendors typically expand and cryopreserve them for dissemination. Building in vitro human liver models with unpassaged hepatocyte-supportive cells is impractical for routine experimentation and cell-based therapy.

Hepatocytes cultured within 3D spheroids can maintain functional outputs long-term compared to 2D monocultures[1]. Although PHH spheroids could maintain stable levels of liver functions here, PFs increased PHH functions in spheroids, suggesting that the PF effect on PHH functions is independent of 2D or 3D culture format, which could be helpful for both in vitro and in vivo applications. However, functions were lower in spheroids than MPCCs when considering the PHH numbers in each platform. This difference requires further investigation but is likely related to the cell ratio and the organization of homotypic/heterotypic

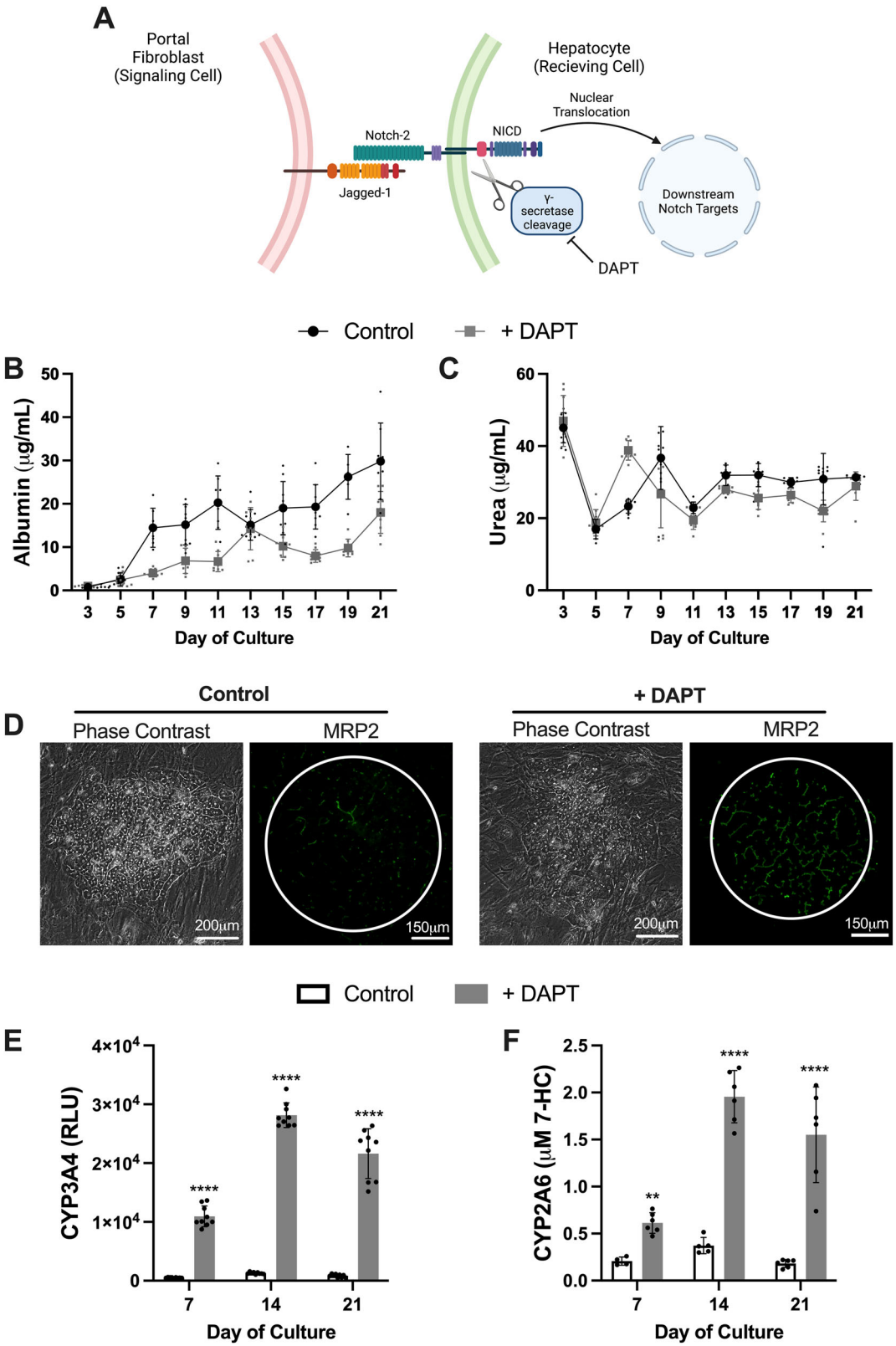

Fig. 9 | The role of Notch signaling in PHH + PF MPCCs. A Notch signaling pathway diagram. Created in BioRender. Khetani, S. (2025) https://BioRender.com/bjz4w91. Notch signaling was inhibited in MPCCs using a gamma-secretase inhibitor, DAPT. Time series of **B** albumin (n = 9 technical replicates) and **C** urea secretions (n = 9) in DAPT-treated versus control MPCCs show that while some transient downregulation of albumin secretion was observed with DAPT treatment, urea secretion was unaffected. **D** Phase contrast and MRP2-immunostained images of MPCCs indicate that while there was no change in morphology, an increase in MRP2 staining was observed in the DAPT-treated cultures. Time series of **E** CYP3A4 enzyme activity (n = 9) and **F** CYP2A6 enzyme activity (n = 6), indicating increased activities in DAPT-treated MPCCs compared to the controls. $^{*}P < 0.05$, $^{***}P < 0.001$, $^{****}P < 0.0001$. Scale bar = 200 μm on the phase contrast images and scale bar = 150 μm on the immunostained images.

interactions across the two models. Indeed, MPCCs functionally outperform randomly distributed cocultures, which have disorganized interactions across the two cell types as in spheroids, in both functions[10] and hepatitis B viral infection kinetics[15].

Interestingly, even though HSCs were subjected to a much softer milieu than plastic in the agarose microwells used to create and house the spheroids, they did not induce PHH functions in spheroids to any considerable degree and, in some cases, caused downregulation relative to the PHH monoculture spheroids. Since the same HSCs induced PHH functions on plastic, their phenotype in spheroids versus on plastic needs further probing to elucidate the differences. Ultimately, it may be possible to make spheroids higher functioning by optimizing their size for nutrient/metabolite diffusion, by sequential cell layering to maintain PHH homotypic contacts while providing a heterotypic interface with the fibroblasts at the spheroid periphery, or by using quiescent HSCs instead of activated ones; however, such optimization is beyond the scope of this study that is focused on studying the interactions between PHHs and liver fibroblasts.

We found that IGFBP5 was expressed at higher levels in PFs than in HSCs, and inhibiting IGFBP5 via siRNA treatment decreased hepatic insulin sensitivity. IGFBP5 is one of six IGFBPs that maintain a role in regulating IGFs by extending their half-life and is the most conserved IGFBP among species[51]. Since the insulin-like growth factor receptor 1 (IGF1R) can form heterodimers with the insulin receptor[52], the increase in the stability of hepatocyte-secreted IGF1/2 by PF-derived IGFBP5 and subsequent binding to IGF1R may underlie the increase in hepatic insulin sensitivity in cocultures; however, further experiments are needed to confirm this hypothesis. Nonetheless, IGFBP5 has been shown to decrease in models of MASLD, and the overexpression of IGFBP5 lowered lipid accumulation, maintained expression of β-oxidation genes, and allowed for maintenance of insulin sensitivity in vitro and in vivo[30].

Although it has been proposed that IGFBP5 may be a profibrotic marker due to its ability to reduce apoptosis in LX-2 (an HSC cell line) and increase production of both ECM secretion and degradation genes[53], overexpression in mouse models prone to biliary fibrosis has shown the opposite effect[39]. In ABCB4$^{-/-}$ mice, a mouse line spontaneously developing biliary fibrosis, overexpression of IGFBP5 led to reduced hepatocyte damage, inflammation, oxidative stress, and overall fibrosis[39]. Similarly, we found here that inhibiting IGFBP5 led to an increase in the expression of α-SMA, indicating that IGFBP5 attenuates PF activation.

Notch signaling is a highly conserved pathway that has been found to control cell fate, morphogenesis, and proliferation[54]. In the liver, Notch signaling is upregulated in the bile duct region. Specifically, PFs express the Notch signaling ligand, Jagged-1, which interacts with bipotential progenitor cells to induce a cholangiocyte phenotype[41]. In vivo, hepatocytes can revert to a distinct progenitor state, expressing both HNF4a and SOX9, that can become either mature hepatocytes or cholangiocytes[55]. Although PFs induced high levels of PHH functions compared to HSCs and PHH monocultures, the cocultured PHHs expressed various progenitor-like markers (i.e., *PTX3*, *CD115*, and *CK19*). This phenomenon is significantly driven by Notch signaling[55]. For example, liver fibroblasts have been shown to aid in the conversion of primary hepatocytes into ductal cells; when Notch signaling was inhibited via treatment with a gamma-secretase inhibitor, the percentage of bipotential (HNF4a+SOX9+) cells was dramatically downregulated in the injured model and in vitro[56]. Therefore, we hypothesized that inhibiting Notch signaling in PHH + PF cocultures with a gamma-secretase inhibitor would reduce the progenitor-like state of the PHHs and boost their adult functions further. Indeed, cocultures treated with two different gamma-secretase small molecule inhibitors (DAPT and Compound E) led to increased hepatic CYP450 activities and improved polarity determined through staining for the transporter MRP2. Even the functions of PHH + HSC cocultures were enhanced similarly with DAPT treatment, suggesting similar underlying mechanisms as the PHH + PF cocultures. This indicates an in vivo-relevant phenomenon in these cocultures, which can be further investigated to improve the functionality and longevity of in vitro liver platforms.

Although the number of PFs relative to PHHs differs in MPCCs and spheroids than in the entire native liver, the ratio of PFs and PHHs in the portal triad region may be higher. Nonetheless, to further address the effects of cell ratios, we growth-arrested PFs and HSCs using mitomycin C and then modulated the PHH to fibroblast ratios in cocultures. PHH functions were induced even when the ratio was reduced to 1 fibroblast to 20 PHHs compared to PHH monocultures. Growth-arrested HSCs induced some PHH functions at similar levels as PFs but not all, suggesting that the difference in the growth rates of the two fibroblast types is not the sole mechanism underlying the differences in the induction of PHH functions. However, PFs at higher passages (>7) lost contact inhibition, secreted higher levels of inflammation marker, IL-6, and induced PHH functions at lower levels than lower passage PFs. This issue could be mitigated significantly by inhibiting TGF-β signaling, suggesting that even higher passage PFs express molecules to support PHHs, which is useful for the routine use of PFs for fabricating liver models for downstream applications.

In conclusion, we show that PFs induced functions in PHHs via paracrine and juxtacrine interactions, partly via IGFBP5 signaling. Inhibiting Notch signaling further enhanced PHH functions by reducing their progenitor-like state in the cocultures. Inhibiting TGF-β signaling suppressed the overgrowth and inflammation in higher passage PFs while still allowing their inductive effects on PHH functions. Overall, our findings provide unique insights into the role of PFs in promoting homeostatic hepatic functions within and around the portal triad. Our 2D and 3D platforms containing PHHs and PFs provide all-human and all-liver strategies for investigations of compound metabolism and toxicity, modeling liver diseases, and as a building block for generating tissue surrogates for cell-based therapies.

Methods

HSC and PF culture

Cryopreserved primary human HSCs (pre-passaged) were obtained from Samsara Sciences (San Diego, CA) and ZenBio (Durham, NC). HSCs were further passaged with media containing 10% (v/v) fetal bovine serum (FBS; Thermo Fisher Scientific, Waltham, MA) with high glucose Dulbecco's Modified Eagle's Medium (DMEM; 11965092, Gibco, Grand Island, NY) and 1% (v/v) penicillin/streptomycin (30-002-CI, Corning, Corning, NY) on poly-L-lysine (PLL, 0403, Sciencell, Carlsbad, CA)-coated flasks (20 μg mL^{-1}). Comparatively, PFs were isolated in-house from the NPC fraction of two liver donors (Lonza, Walkersville, MD) subjected to Percoll-based separations. Percoll (GE17-0891-01, GE Healthcare, Chicago, IL) was diluted to 25% (v/v) and 50% (v/v) stocks in 1× phosphate-buffered saline (PBS; 46-013-CM, Corning). Briefly, the NPC fraction was divided into 50 mL portions and centrifuged at 300 × *g* for 20 min. The supernatant from each portion was removed, and the remaining suspension was stacked above a top layer of 20 mL 25% (v/v) Percoll and a bottom layer of 15 mL 50% (v/v) Percoll. This column was centrifuged at 900 × *g* for 25 min without a brake on the centrifuge. The top layer was removed and discarded, while the layer between 10 mL and 20 mL was mixed with 25 mL 1× PBS and centrifuged at 300 × *g* for 20 min. The resulting cell pellet was resuspended in the culture medium and incubated on a tissue culture polystyrene flask for 10 min at 37 °C and 10% CO_2 to separate Kupffer cells. The resulting PFs in the supernatant of the previous dish were moved to another tissue culture flask for expansion and coculture. PFs were passaged with media containing 10% (v/v) FBS with high glucose DMEM and 1% (v/v) penicillin/streptomycin. HSCs and PFs were commercially obtained from de-identified donors, whose information is shown in Table 1 as available from the vendors.

PHH and fibroblast cocultures

Adsorbed rat tail collagen I (354236, Corning) was patterned lithographically in each well of a 24-well plate to create 500 μm diameter circular domains spaced 1200 μm apart measuring center-to-center[19]. PHHs selectively attached to the collagen domains, leading to ~30,000 attached PHHs

Table 1 | Donor demographics

Cell type	Vendor	Lot	Sex	Race	Age
PF	Lonza	HUM4054	Female	Caucasian	23
PF	Lonza	NA	NA	NA	NA
HSC	Samsara	170063	NA	NA	NA
HSC	Samsara	150002	Male	AA	24
HSC	ZenBio	022113	Male	Caucasian	58
HSC	ZenBio	101915CC	Male	Caucasian	18
PHH	Lonza	HUM4055A	Female	Caucasian	54
PHH	Lonza	HUM4145	Male	Caucasian	2
PHH	Lonza	HUM4192	Female	Asian	16
PHH	Novabiosis	Lot10	Male	Caucasian	2

AA African American, *NA* not available from the vendor.

on ~90 collagen-coated islands in each well of a 24-well plate. PHHs were commercially obtained from de-identified donors, whose information is shown in Table 1 as available from the vendors. PFs or HSCs were then seeded 18 to 24 h later at ~90,000 cells per well to create a coculture. Micropatterned hepatocyte monocultures without fibroblasts were used as density-matched controls. Hepatocyte culture medium containing a 5 mM glucose DMEM (Corning) base supplemented with 15 mM HEPES [4-(2-hydroxyethyl)-1-piperazineethane-sulfonic acid] buffer (25-060-CI, Corning), 1% (v/v) penicillin/streptomycin, TS+ (6.25 μg mL^{-1} transferrin, 6.25 ng mL^{-1} selenous acid, 5.35 μg mL^{-1} linoleic acid, bovine serum albumin), 20 nM insulin, 7 ng mL^{-1} glucagon (G2044, Sigma-Aldrich, St. Louis, MO) and 0.1 μM dexamethasone (D4902, Sigma-Aldrich) was replaced every 2 days (300 μL/well for 24-well plate)[19]. PFs or HSCs were used between passages 5 to 9 for all coculture studies, apart from the passage dependence PF study where PFs up to passage 11 were utilized.

Molten agarose (2% (m/v), A9539, Sigma-Aldrich) was prepared and dispensed into each well of a 24-well tissue culture[57]. PDMS stamps with ~1000 micropillars were placed into molten agarose within each well of a 24-well tissue culture plate. After the agarose was allowed to cool, the PDMS stamps were removed, leaving behind ~300 μm diameter by ~300 μm deep wells cast in agarose. The microwells were sterilized with 70% (v/v) ethanol before cell seeding. PHHs were seeded into the microwells, and PFs or HSCs were seeded within 24 h at a 1:1 ratio with PHHs (150K cells/well for each cell type) to form 3D spheroids. For PHH-only spheroids, 200K cells were seeded into the microwells. Culture media changes (300 μL/well) were performed every 48 h. The same medium formulation as above for MPCCs was used for spheroids.

For PF-conditioned medium experiments, PHHs were seeded into micropatterns as described above. Subsequently, ~90,000 PFs/well were seeded in additional wells of a 24-well plate. After 48 h, the medium was collected from the PF wells, sterile-filtered, and added to the PHH micropatterns; control (non-conditioned) media was used on some PHHs. This procedure was repeated every 48 h.

Knockdown of gene expression

PHH + PF MPCCs were allowed 7 days to stabilize and then treated with 10 pmol ON-TARGET plus small interfering (si)RNA against human IGFBP5 (L-010897-00-0005, Horizon Discovery, Cambridge, United Kingdom) or 10 pmol scrambled siRNA control (Silencer, 4390843, Invitrogen, Waltham, MA) with lipofectamine RNAiMAX (13778100, Thermo Fisher) per the manufacturer's instructions. Briefly, the siRNA and the lipofectamine RNAiMAX were diluted separately in Opti-MEM media (31985062, Thermo Fisher), combined at a 1:1 ratio, and incubated for 5 min at room temperature (RT). The siRNA-lipid complex was then added to the cells dropwise and incubated for 48 h, followed by a culture medium change. Following the manufacturer's protocol, gene expression knockdown was assessed utilizing an enzyme-linked immunosorbent assay (ELISA) against IGFBP5 (DY875, R&D Systems, Minneapolis, MN).

Notch signaling inhibition

PHH + PF MPCCs were treated with 25 μM *N*-[*N*-(3,5-Difluorophenacetyl)-L-alanyl]-*S*-phenylglycine *t*-butyl ester (DAPT, 13197, Cayman Chemical Company, Ann Arbor, MI), a gamma-secretase inhibitor, dissolved in dimethyl-sulfoxide (DMSO) every other day for 21 days. Cocultures treated with only DMSO as a vehicle control were also maintained. Immunostaining and gene expression results were obtained on day 21. Results were verified with an additional gamma-secretase inhibitor, compound E, at 25 μM (15579, Cayman Chemical).

Immunostaining

Cultures were fixed in a 4% (v/v) paraformaldehyde solution (Alfa Aesar, Haverhill, MA) for 15 min at RT and rinsed three times with 1× PBS. The cultures were then permeabilized and blocked utilizing 0.3% (v/v) Triton X-100 (Amresco, Solon, OH) with 1% (m/v) donkey serum (SouthernBiotech, Birmingham, AL) in 1× PBS for 45 min at RT. Primary antibodies, including mouse anti-human α-smooth muscle actin (α-SMA, MAB1420, Mouse, 1:200, R&D Systems), rabbit anti-human fibulin-2 (PA5-51665, Rabbit, 1:200, Invitrogen), sheep anti-human collagen 1α1 (AF6220, Sheep, 1:200, R&D Systems), rabbit anti-human albumin (109-433, Rabbit, 1:200, Rockland Immunochemicals), and mouse anti-human MRP2 (SC59608, Mouse, 1:200, Santa Cruz Biotechnology), mouse anti-CD31 (3528, Mouse, 1:200, Cell Signaling Technology), and mouse anti-CD68 (556059, Mouse, 1:200, BD Biosciences) were added with buffer containing 0.3% (v/v) Triton X-100 (97063-864, VWR, Radnor, PA) with 0.1% (m/v) bovine serum albumin (BSA, BP1600-100, Thermo Fisher) and were incubated overnight at 4 °C. The cultures were then rinsed three times with 1× PBS and labeled with Alexa Fluor 647 donkey anti-mouse IgG (A-31571, Invitrogen), Alexa Fluor 568 donkey anti-rabbit IgG (A10042, Invitrogen), Alexa Fluor 488 goat anti-rabbit IgG (A-11008, Invitrogen), or Alexa Fluor 488 goat anti-sheep IgG (A-11015, Invitrogen) for 1 h at 37 °C, with DAPI (4′,6-diamidino-2-phenylindole) (D1306, Invitrogen) added for the final 15 min. Finally, the cultures were washed three times with 1× PBS and imaged using an epifluorescence Olympus IX83 automated microscope (Evident Scientific, Waltham, MA) equipped with a Hamamatsu Flash 4.0LT+sCMOS camera (Hamamatsu USA, Bridgewater, NJ).

Morphological and functional assessments

Culture morphology was assessed using an EVOS M5000 imaging system with phase contrast objectives (AMF5000, Thermo Fisher). Culture supernatants were assayed for urea concentration utilizing a colorimetric endpoint assay using diacetyl monoxime with acid and heat (SB-0580-250, Stanbio Labs, Boerne, TX)[10]. Albumin concentration was determined by assaying culture supernatants using a competitive ELISA (0855235, MP Biomedicals, Santa Ana, CA) with horseradish peroxidase detection and 3, 3′, 5,5′-tetramethylbenzidine (TMB; TMBE-100, Rockland Immunochemicals) as the substrate[10]. CYP3A4 and CYP2C9 enzyme activities were assessed by incubating the cultures with substrates (luciferin-IPA for CYP3A4, V9002, and luciferin-H for CYP2C9, V8792, from Promega Life Sciences, Madison, WI) for 1 h and 3 h, respectively, at 37 °C and then detecting the luminescence of the metabolite produced (luciferin) according to the manufacturer's protocols. CYP1A2 and CYP2A6 activities were measured by incubating cultures with 5 μM 7-ethoxyresorufin (E3763, Sigma-Aldrich, St. Louis, MO) for 3 h or 50 μM coumarin (C4261, Sigma-Aldrich) for 1 h, respectively. The metabolites, resorufin and 7-hydroxycoumarin (7-HC), were quantified via fluorescence on a Biotek Synergy H1 multi-mode plate reader (excitation/emission (nm): 550/585 for resorufin, and 355/460 for 7-HC).

Insulin sensitivity/resistance was assessed by incubating cultures with a hormone-free culture medium for 24 h. Cultures were then washed three times with 1× PBS to remove the remaining glucose and then incubated for 6 h with a glucose-free medium containing 4 mM L-glutamine, 1% (v/v) penicillin/streptomycin, 1.5% (v/v) HEPES buffer, gluconeogenic substrates, 20 mM lactate (71720-25G, Sigma-Aldrich) and 2 mM pyruvate (P2256-25G, Sigma-Aldrich), and with or without 10 nM insulin. The supernatants were collected and assayed for glucose via an Amplex Red

glucose/glucose oxidase kit (A22189, Thermo Fisher). Insulin sensitivity was calculated by dividing the insulin-inhibited glucose output by the basal level of glucose output in the absence of insulin.

Gene expression analysis

For bulk RNA sequencing and quantitative polymerase chain reaction (qPCR) analysis, RNA was extracted from cultures with TRIzol (15596026, Ambion, Austin, TX) and purified with the RNeasy kit (74104, Qiagen, Germantown, MD). Genomic DNA was removed from the purified RNA with a DNase I treatment (M0303S, New England Biolabs, Ipswich, MA) for 10 min.

The complementary DNA (cDNA) was synthesized with the AzuraFlex cDNA Synthesis Kit (AZ-1997, Azura Genomics, Raynham, MA). The cDNA was added along with either Taqman master mix (4304437, Thermo Fisher) or PowerUp SYBR green master mix (A25742, Applied Biosystems, Waltham, MA) as well as either predesigned Taqman human-specific primer/probe sets (Thermo Fisher) or generated primer sequences (Integrated DNA Technologies, Coralville, IA). Primer information for generated primer sequences can be found in Supplementary Table 1. Reported gene expression values were calculated as fold change relative to the denoted control using the $\Delta\Delta C_T$ method with glyceraldehyde 3-phosphate dehydrogenase (GAPDH) or β-actin as the housekeeping genes.

RNA sequencing was performed using Illumina NovaSeq 6000 at the University of Chicago Genomics Facility. All conclusions were based on two donors of PFs and two donors of HSCs. Data alignment to the human genome was performed utilizing BioJupies with the default parameter settings[58]. The R package edgeR (version 3.34.1) was used for count normalization and differential expression analysis[59]. The adjusted *P*-value was calculated utilizing the p.adjust function in edgeR. Reactome pathway analysis was performed in Cytoscape using the ClueGo package for analysis and visualization[60].

Statistics and reproducibility

All experimental findings were validated in 2–3 independent experiments, with 3+ replicate wells per experiment, from at least two cryopreserved PHH donors, two PF donors, and two HSC donors. Data was visualized and analyzed using Microsoft Excel and GraphPad Prism (La Jolla, CA). Mean, standard deviation, and individual data points are displayed for all data sets. Statistical significance was determined using Student's *t*-test or two-way ANOVA followed by a Bonferroni pair-wise post-hoc test ($P < 0.05$).

Data availability

All data are available in the main text or Supplementary Materials. The source data for the graphs are provided in the Supplementary Microsoft Excel file labeled "Supplementary Data." RNA sequencing results can be found in the Gene Expression Omnibus (GEO) database with the accession number GSE289290.

Received: 12 May 2024; Accepted: 25 April 2025;
Published online: 09 May 2025

References

1. Monckton, C. P., Brown, G. E. & Khetani, S. R. Latest impact of engineered human liver platforms on drug development. *APL Bioeng.* **5**, 031506 (2021).
2. Kukla, D. A. & Khetani, S. R. Bioengineered liver models for investigating disease pathogenesis and regenerative medicine. *Semin Liver Dis.* **41**, 368–392 (2021).
3. Shan, J. et al. Identification of small molecules for human hepatocyte expansion and iPS differentiation. *Nat. Chem. Biol.* **9**, 514–520 (2013).
4. Kim, Y. et al. Small molecule-mediated reprogramming of human hepatocytes into bipotent progenitor cells. *J. Hepatol.* **70**, 97–107 (2019).
5. Zaret, K. S. Regulatory phases of early liver development: paradigms of organogenesis. *Nat. Rev. Genet.* **3**, 499–512 (2002).
6. Langenbach, R. et al. Maintenance of adult rat hepatocytes on C3H/10T1/2 cells. *Cancer Res.* **39**, 3509–3514 (1979).
7. Guguen-Guillouzo, C. et al. Maintenance and reversibility of active albumin secretion by adult rat hepatocytes co-cultured with another liver epithelial cell type. *Exp. Cell Res.* **143**, 47–54 (1983).
8. Clement, B. et al. Long-term co-cultures of adult human hepatocytes with rat liver epithelial cells: modulation of albumin secretion and accumulation of extracellular material. *Hepatology* **4**, 373–380 (1984).
9. Khetani, S. R., Szulgit, G., Del Rio, J. A., Barlow, C. & Bhatia, S. N. Exploring interactions between rat hepatocytes and nonparenchymal cells using gene expression profiling. *Hepatology* **40**, 545–554 (2004).
10. Khetani, S. R. & Bhatia, S. N. Microscale culture of human liver cells for drug development. *Nat. Biotechnol.* **26**, 120–126 (2008).
11. Chan, T. S., Yu, H., Moore, A., Khetani, S. R. & Tweedie, D. Meeting the challenge of predicting hepatic clearance of compounds slowly metabolized by cytochrome P450 using a novel hepatocyte model, HepatoPac. *Drug Metab. Dispos.* **47**, 58–66 (2019).
12. Wang, W. W., Khetani, S. R., Krzyzewski, S., Duignan, D. B. & Obach, R. S. Assessment of a micropatterned hepatocyte coculture system to generate major human excretory and circulating drug metabolites. *Drug Metab. Dispos.* **38**, 1900–1905 (2010).
13. Khetani, S. R. et al. Use of micropatterned cocultures to detect compounds that cause drug-induced liver injury in humans. *Toxicol. Sci.* **132**, 107–117 (2013).
14. Ploss, A. et al. Persistent hepatitis C virus infection in microscale primary human hepatocyte cultures. *Proc. Natl. Acad. Sci. USA* **107**, 3141–3145 (2010).
15. Shlomai, A. et al. Modeling host interactions with hepatitis B virus using primary and induced pluripotent stem cell-derived hepatocellular systems. *Proc. Natl. Acad. Sci. USA* **111**, 12193–12198 (2014).
16. March, S. et al. Micropatterned coculture of primary human hepatocytes and supportive cells for the study of hepatotropic pathogens. *Nat. Protoc.* **10**, 2027–2053 (2015).
17. Davidson, M. D., Kukla, D. A. & Khetani, S. R. Microengineered cultures containing human hepatic stellate cells and hepatocytes for drug development. *Integr. Biol.* **9**, 662–677 (2017).
18. Davidson, M. D., Ballinger, K. R. & Khetani, S. R. Long-term exposure to abnormal glucose levels alters drug metabolism pathways and insulin sensitivity in primary human hepatocytes. *Sci. Rep.* **6**, 28178 (2016).
19. Ware, B. R., Durham, M. J., Monckton, C. P. & Khetani, S. R. A cell culture platform to maintain long-term phenotype of primary human hepatocytes and endothelial cells. *Cell. Mol. Gastroenterol. Hepatol.* **5**, 187–207 (2018).
20. Nguyen, T. V. et al. Establishment of a hepatocyte-Kupffer cell coculture model for assessment of proinflammatory cytokine effects on metabolizing enzymes and drug transporters. *Drug Metab. Dispos.* **43**, 774–785 (2015).
21. Stevens, K. R. et al. In situ expansion of engineered human liver tissue in a mouse model of chronic liver disease. *Sci. Transl. Med.* **9**, https://doi.org/10.1126/scitranslmed.aah5505 (2017).
22. Weaver, J. R. et al. The morphology, functionality, and longevity of a novel all human hepatic cell-based tri-culture system. *Toxicol. Vitr.* **86**, 105504 (2023).
23. Wells, R. G. The portal fibroblast: not just a poor man's stellate cell. *Gastroenterology* **147**, 41–47 (2014).
24. Hofmann, J. J. et al. Jagged1 in the portal vein mesenchyme regulates intrahepatic bile duct development: insights into Alagille syndrome. *Development* **137**, 4061–4072 (2010).
25. Dranoff, J. A. & Wells, R. G. Portal fibroblasts: underappreciated mediators of biliary fibrosis. *Hepatology* **51**, 1438–1444 (2010).
26. Kanta, J. Elastin in the liver. *Front. Physiol.* **7**, 491 (2016).
27. Li, Z. et al. Transforming growth factor-beta and substrate stiffness regulate portal fibroblast activation in culture. *Hepatology* **46**, 1246–1256 (2007).

28. Cangemi, C., Hansen, M. L., Argraves, W. S. & Rasmussen, L. M. Fibulins and their role in cardiovascular biology and disease. *Adv. Clin. Chem.* **67**, 245–265 (2014).
29. Mohan, S. & Baylink, D. J. IGF-binding proteins are multifunctional and act via IGF-dependent and -independent mechanisms. *J. Endocrinol.* **175**, 19–31 (2002).
30. Xiao, Z., Chu, Y. & Qin, W. IGFBP5 modulates lipid metabolism and insulin sensitivity through activating AMPK pathway in non-alcoholic fatty liver disease. *Life Sci.* **256**, 117997 (2020).
31. Fuji, H. et al. The role of Mesothelin signaling in Portal Fibroblasts in the pathogenesis of cholestatic liver fibrosis. *Front. Mol. Biosci.* **8**, 790032 (2021).
32. Karin, D., Koyama, Y., Brenner, D. & Kisseleva, T. The characteristics of activated portal fibroblasts/myofibroblasts in liver fibrosis. *Differentiation* **92**, 84–92 (2016).
33. Olsen, A. L. et al. Hepatic stellate cells require a stiff environment for myofibroblastic differentiation. *Am. J. Physiol. Gastrointest. Liver Physiol.* **301**, G110–G118 (2011).
34. LeCluyse, E. L., Witek, R. P., Andersen, M. E. & Powers, M. J. Organotypic liver culture models: meeting current challenges in toxicity testing. *Crit. Rev. Toxicol.* **42**, 501–548 (2012).
35. Kukla, D. A., Crampton, A. L., Wood, D. K. & Khetani, S. R. Microscale collagen and fibroblast interactions enhance primary human hepatocyte functions in three-dimensional models. *Gene Expr.* **20**, 1–18 (2020).
36. Zhang, J. et al. SB431542-loaded liposomes alleviate liver fibrosis by suppressing TGF-beta signaling. *Mol. Pharm.* **17**, 4152–4162 (2020).
37. Santoleri, D. & Titchenell, P. M. Resolving the paradox of hepatic insulin resistance. *Cell. Mol. Gastroenterol. Hepatol.* **7**, 447–456 (2019).
38. Davidson, M. D., Lehrer, M. & Khetani, S. R. Hormone and drug-mediated modulation of glucose metabolism in a microscale model of the human liver. *Tissue Eng. Part C Methods* **21**, 716–725 (2015).
39. Sokolovic, A. et al. Overexpression of insulin like growth factor binding protein 5 reduces liver fibrosis in chronic cholangiopathy. *Biochim. Biophys. Acta* **1822**, 996–1003 (2012).
40. Suzuki, K. et al. p75 Neurotrophin receptor is a marker for precursors of stellate cells and portal fibroblasts in mouse fetal liver. *Gastroenterology* **135**, 270–281 e273 (2008).
41. Adams, J. M. & Jafar-Nejad, H. The roles of notch signaling in liver development and disease. *Biomolecules* **9**, https://doi.org/10.3390/biom9100608 (2019).
42. Boulter, L. et al. Macrophage-derived Wnt opposes Notch signaling to specify hepatic progenitor cell fate in chronic liver disease. *Nat. Med* **18**, 572–579 (2012).
43. Rizwan, M. et al. Viscoelastic notch signaling hydrogel induces liver bile duct organoid growth and morphogenesis. *Adv. Health. Mater.* **11**, e2200880 (2022).
44. Dobie, R. et al. Single-cell transcriptomics uncovers zonation of function in the mesenchyme during liver fibrosis. *Cell Rep.* **29**, 1832–1847.e8 (2019).
45. Allard, J. B. & Duan, C. IGF-binding proteins: why do they exist and why are there so many?. *Front. Endocrinol.* **9**, 117 (2018).
46. Krause, P., Saghatolislam, F., Koenig, S., Unthan-Fechner, K. & Probst, I. Maintaining hepatocyte differentiation in vitro through co-culture with hepatic stellate cells. *Vitr. Cell. Dev. Biol. Anim.* **45**, 205–212 (2009).
47. Riccalton-Banks, L., Liew, C., Bhandari, R., Fry, J. & Shakesheff, K. Long-term culture of functional liver tissue: three-dimensional coculture of primary hepatocytes and stellate cells. *Tissue Eng.* **9**, 401–410 (2003).
48. Thomas, R. J. et al. The effect of three-dimensional co-culture of hepatocytes and hepatic stellate cells on key hepatocyte functions in vitro. *Cells Tissues Organs* **181**, 67–79 (2005).
49. Mederacke, I. et al. Fate tracing reveals hepatic stellate cells as dominant contributors to liver fibrosis independent of its aetiology. *Nat. Commun.* **4**, 2823 (2013).
50. Kinnman, N. & Housset, C. Peribiliary myofibroblasts in biliary type liver fibrosis. *Front. Biosci.* **7**, D496–D503 (2002).
51. Beattie, J., Allan, G. J., Lochrie, J. D. & Flint, D. J. Insulin-like growth factor-binding protein-5 (IGFBP-5): a critical member of the IGF axis. *Biochem. J.* **395**, 1–19 (2006).
52. Menting, J. G. et al. Structural congruency of ligand binding to the insulin and insulin/type 1 insulin-like growth factor hybrid receptors. *Structure* **23**, 1271–1282 (2015).
53. Sokolovic, A., Sokolovic, M., Boers, W., Elferink, R. P. & Bosma, P. J. Insulin-like growth factor binding protein 5 enhances survival of LX2 human hepatic stellate cells. *Fibrogenes. Tissue Repair* **3**, 3 (2010).
54. Zhou, B. et al. Notch signaling pathway: architecture, disease, and therapeutics. *Signal Transduct. Target Ther.* **7**, 95 (2022).
55. Tarlow, B. D. et al. Bipotential adult liver progenitors are derived from chronically injured mature hepatocytes. *Cell Stem Cell* **15**, 605–618 (2014).
56. Xu, T. et al. Myofibroblast induces hepatocyte-to-ductal metaplasia via laminin-avbeta6 integrin in liver fibrosis. *Cell Death Dis.* **11**, 199 (2020).
57. Cummins, K. A., Crampton, A. L. & Wood, D. K. A high-throughput workflow to study remodeling of ECM-based microtissues. *Tissue Eng. Part C Methods*, https://doi.org/10.1089/ten.TEC.2018.0290 (2018).
58. Torre, D., Lachmann, A. & Ma'ayan, A. BioJupies: automated generation of interactive notebooks for RNA-Seq data analysis in the Cloud. *Cell Syst.* **7**, 556–561.e553 (2018).
59. Robinson, M. D., McCarthy, D. J. & Smyth, G. K. edgeR: a Bioconductor package for differential expression analysis of digital gene expression data. *Bioinformatics* **26**, 139–140 (2010).
60. Bindea, G. et al. ClueGO: a Cytoscape plug-in to decipher functionally grouped gene ontology and pathway annotation networks. *Bioinformatics* **25**, 1091–1093 (2009).

Acknowledgements

We want to thank the University of Chicago Genomics Facility (RRID: SCR019196), especially Dr. Pieter Faber, for their assistance with RNA-seq. Funding was provided by a US National Science Foundation grant CBET-1351909 (S.R.K.) and a National Institutes of Health grant R21ES033528 (S.R.K.).

Author contributions

Conceptualization: G.E.B., V.V.B., B.R.W., S.R.K.; methodology: G.E.B., V.V.B., B.R.W., S.R.K.; investigation: G.E.B., V.V.B., B.R.W.; supervision: S.R.K.; writing—original draft: G.E.B., S.R.K.; writing—review and editing: G.E.B., V.V.B., B.R.W., S.R.K.

Competing interests

The authors declare no competing interests.

Additional information

Supplementary information The online version contains supplementary material available at https://doi.org/10.1038/s42003-025-08135-3.

Correspondence and requests for materials should be addressed to Salman R. Khetani.

Peer review information *Communications Biology* thanks the anonymous reviewers for their contribution to the peer review of this work. Primary Handling Editor: Ophelia Bu.